Experimental methods to examine the structure of melts and glasses

D. V. Louzguine

WPI-AIMR, Tohoku University, Japan

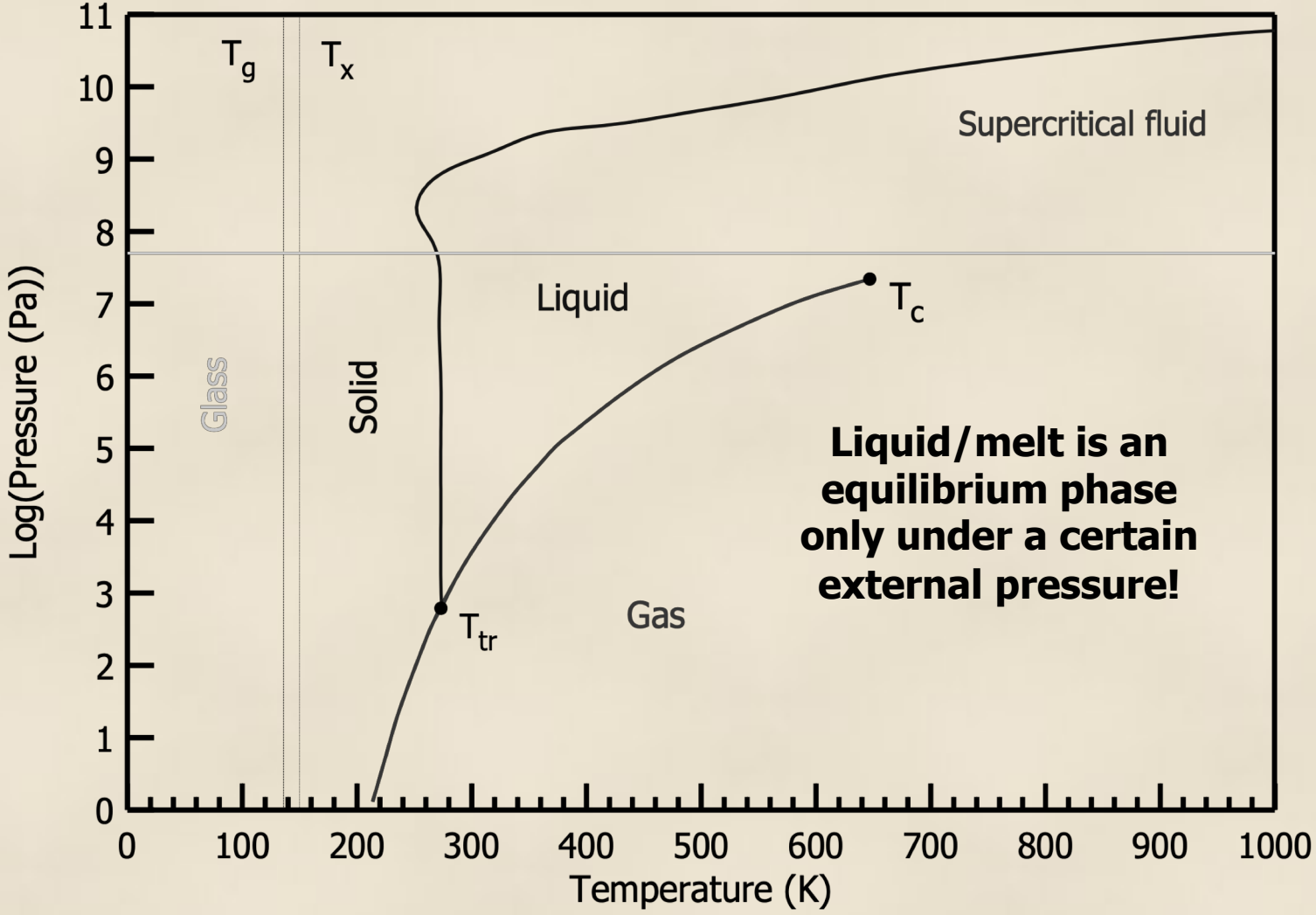

Solid – Liquid – Gas - Plasma

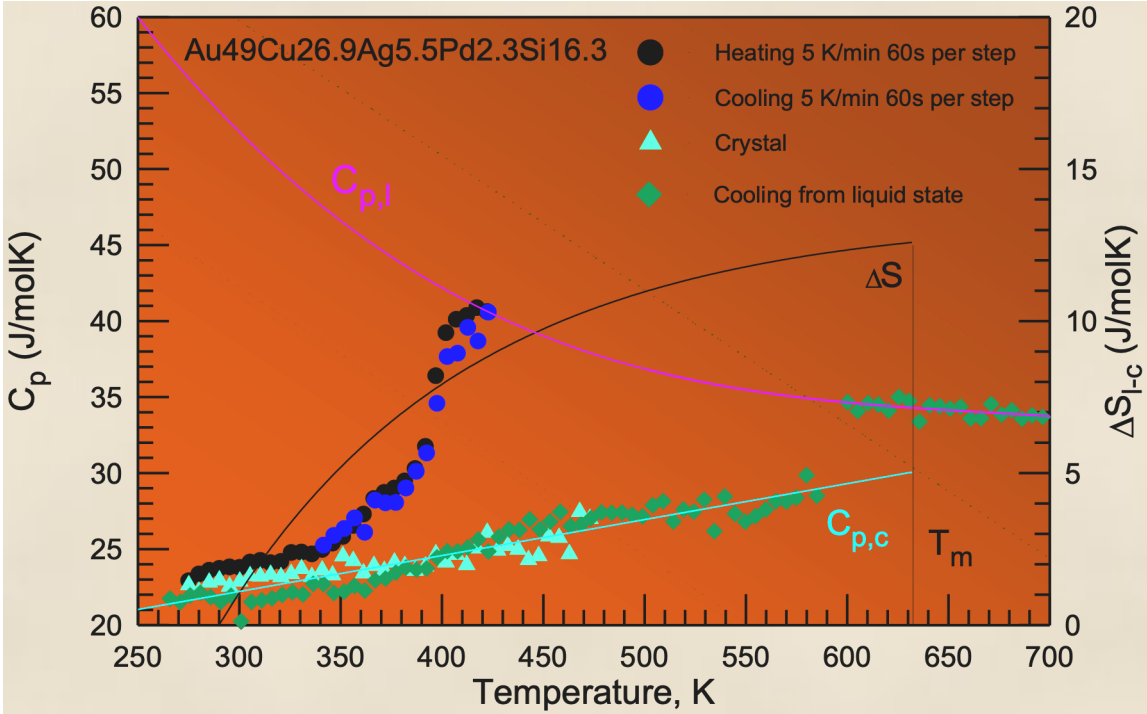

C_p changes steeply at T_g

T_g depends on the cooling rate and on the thermal history

$$\frac{dT_f}{dT}(T) = \frac{C_p(T) - C_{pg}(T)}{C_{pl}(T_f) - C_{pg}(T_f)}$$

$$\Delta S^{l-x}(T) = \Delta S_f - \int_T^{T_m} \frac{c_p^l(T) - c_p^x(T)}{T} dT$$

$$H(T) = H_e(T_f) - \int_T^{T_f} C_{pg}\, dT'$$

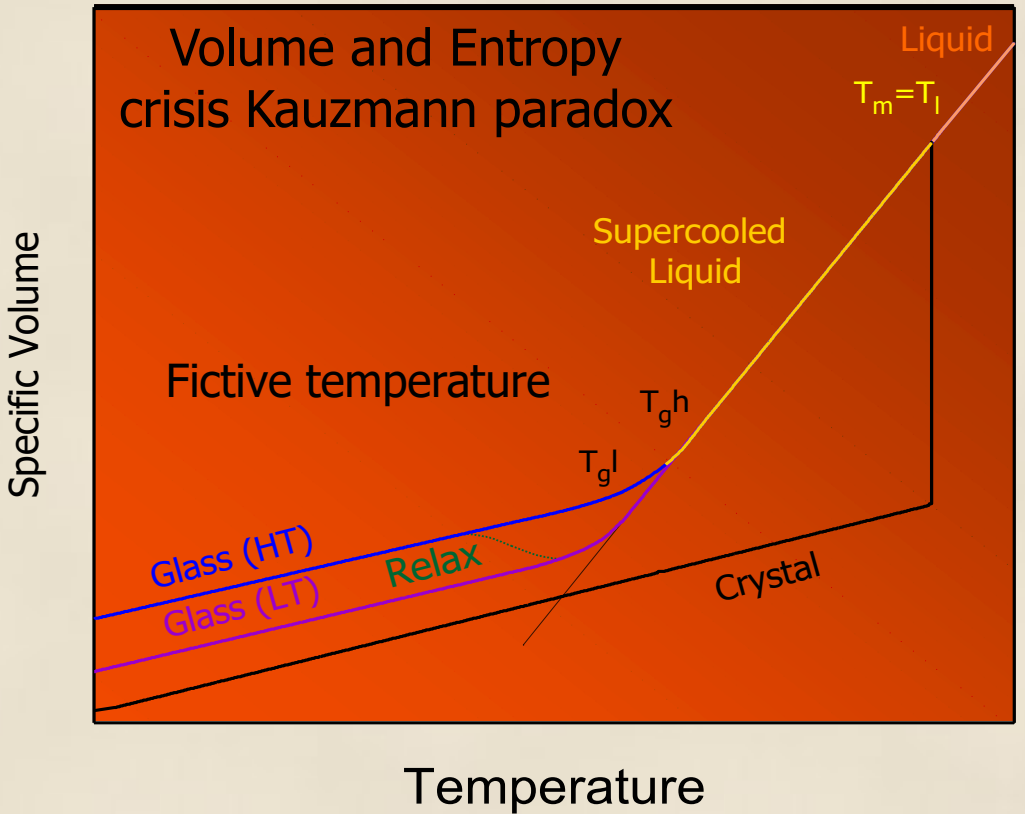

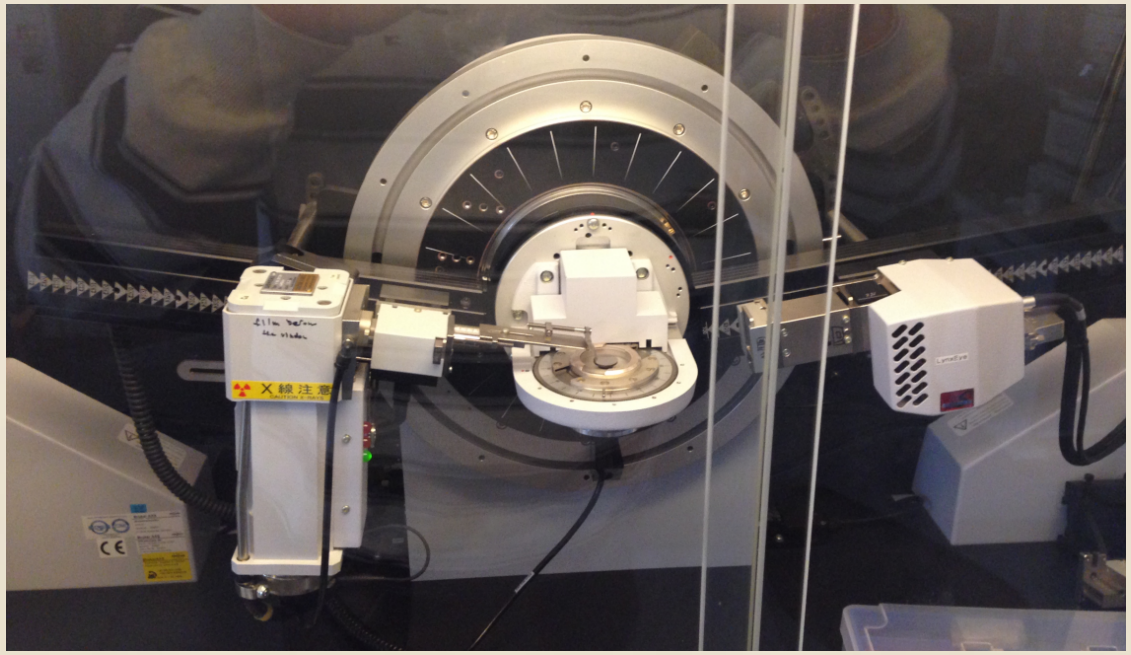

Wavelength ~ d
X-ray diffractometry

For crystals $2d_{hkl}\sin\theta = n\lambda$
θ-diffraction angle
λ-wavelength of X-Rays
n-integer d_{hkl}-spacing

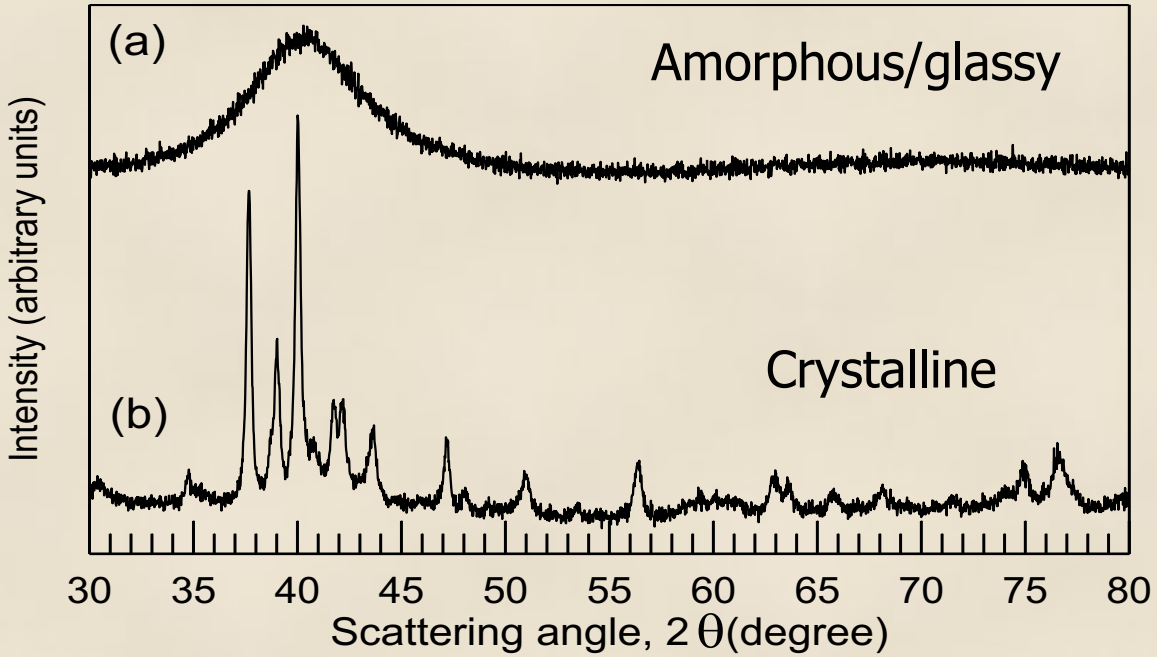

Glassy Short-range order. No translational periodicity

Crystalline. Long-range order and translational periodicity

Structural changes upon glass-transition

In-situ studies of glass-transition by synchrotron XRD. Reciprocal and Real-space functions.

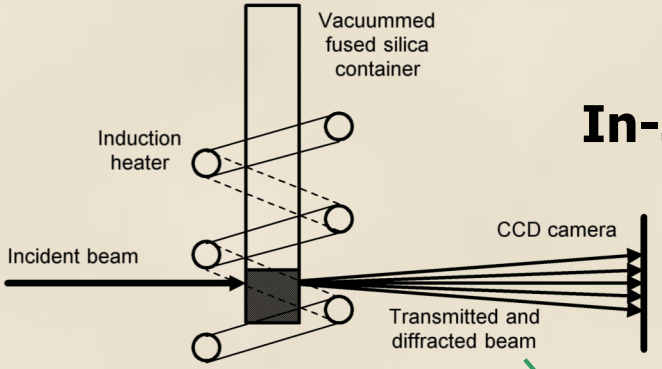

$$RDF(r) = 4\pi r^2 \rho(r) = 4\pi r^2 \rho_0 + 2r/\pi \int_0^{Qmax} QQi(Q)\sin(Qr)dQ$$

Integration of the diffraction pattern

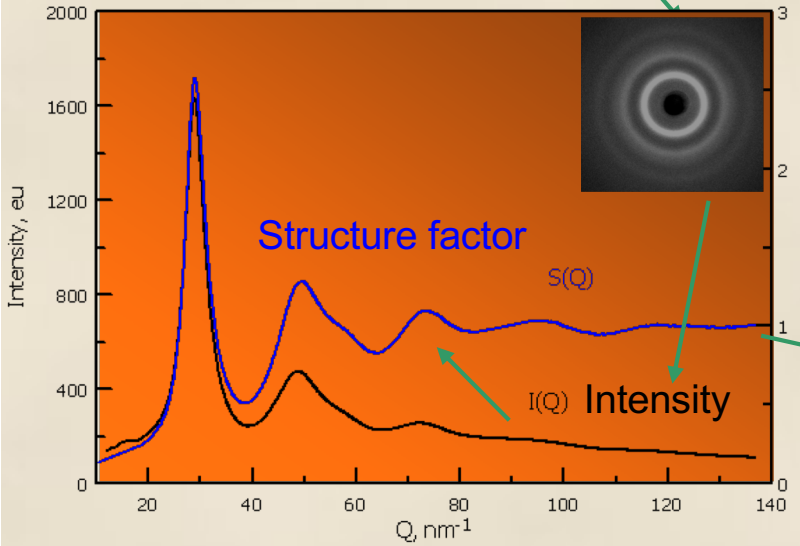

The structure of glasses remains not fully understood. Crystals have unit cells. What are the structural units of glasses?

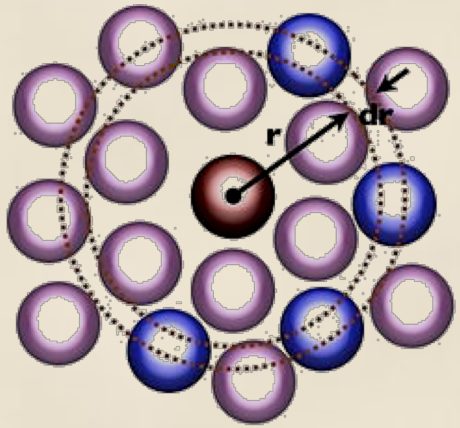

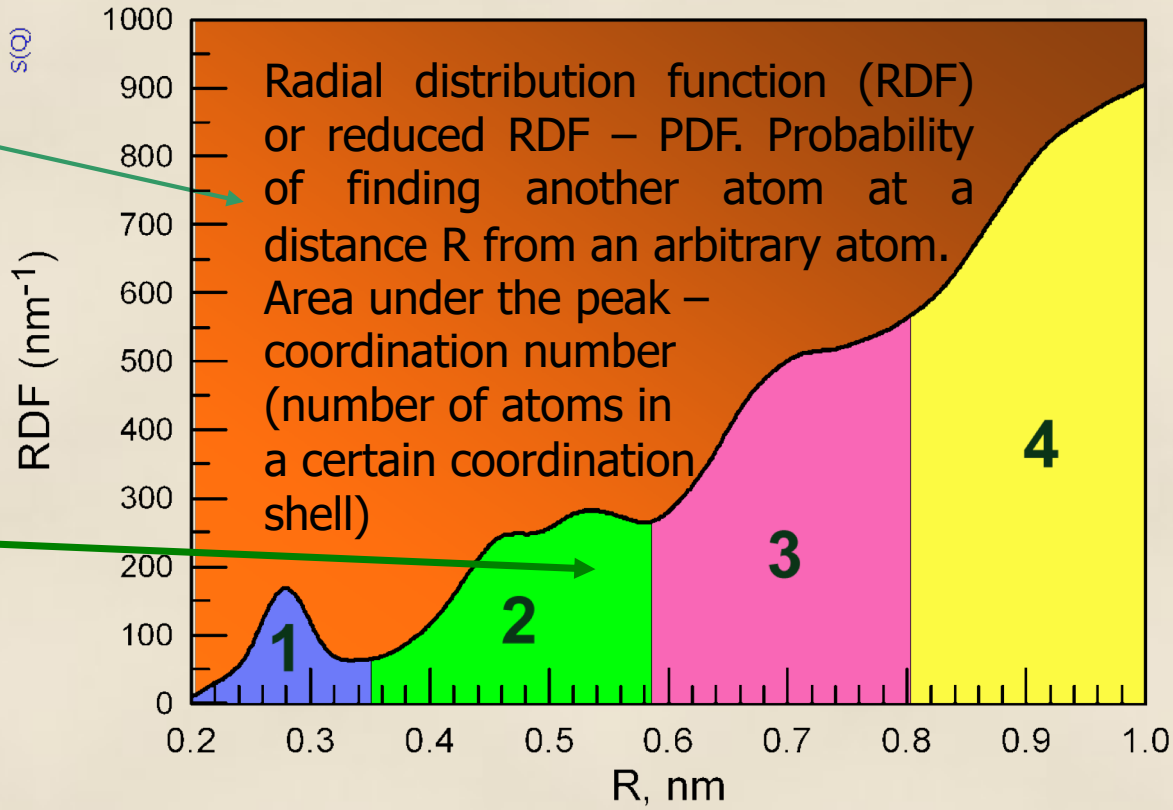

1. Correction for the scattering from the sample container, air scattering, polarization, absorption, and Compton scattering

2. Converted to electron units per atom with the generalized Krogh-Moe-Norman method, using the X-ray atomic scattering factors and anomalous dispersion corrections.

3. The total structure factor S(Q) and the interference function $Q_i(Q)$ ($Q = 4\pi\sin\theta/\lambda$, θ is the diffraction angle) are obtained from the coherent scattering intensity by using atomic scattering factors). The values of $Q_i(Q)$ less than 18 nm^{-1} are smoothly extrapolated to Q=0.

4. The radial distribution RDF(R) and pair distribution functions PDF(R) are obtained by the Fourier transform:

$$4\pi r^2\rho(r) = 4\pi r^2\rho_0 + 2r/\pi \int_0^{Qmax} Q(S(Q)-1)\sin(Qr)dQ$$

where $\rho(r)$ is the total radial number density function and ρ_0 is the average number density of the sample.

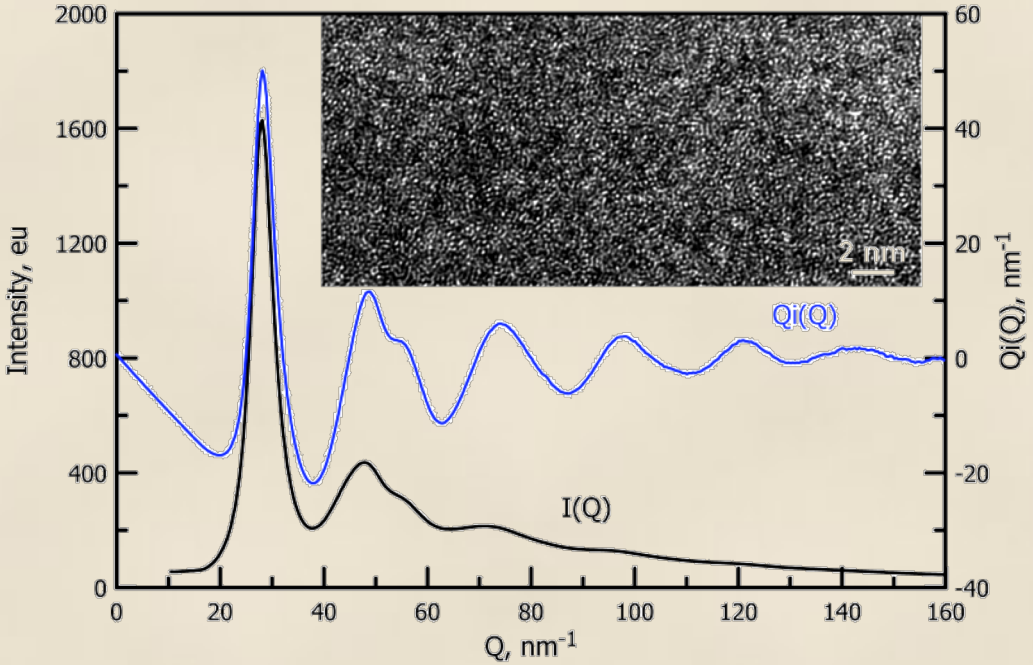

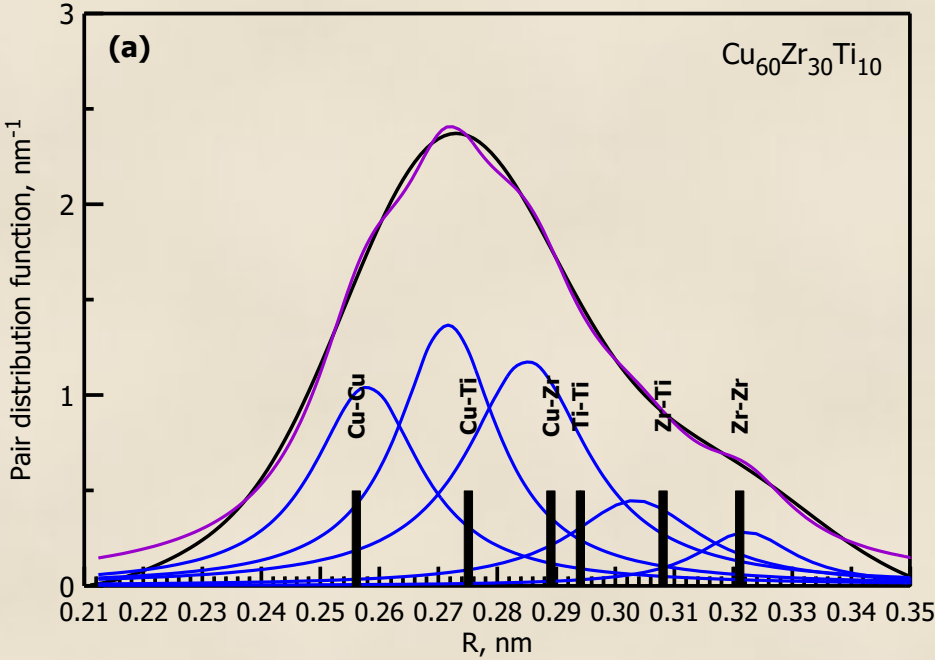

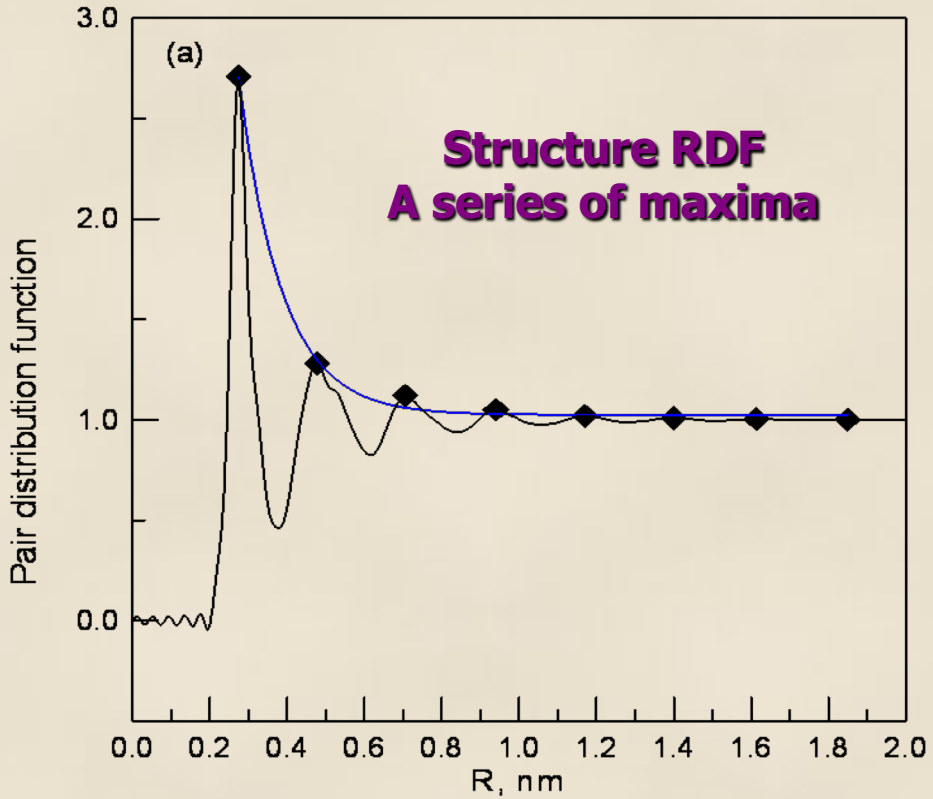

$$4\pi r^2\rho(r) = 4\pi r^2\rho_0 + 2r/\pi \int_0^{kmax} Qi(k)\sin(kr)dk$$

D. V. Louzguine-Luzgin, J. Antonowicz, K. Georgarakis, G. Vaughan, A. R. Yavari and A. Inoue, "Real-space structural studies of Cu-Zr-Ti glassy alloy" Journal of Alloys and Compounds, Vol. 466, N: 1-2, (2008) pp. 106-110.

X-rays interact primarily with the electron cloud surrounding each atom. The contribution to the diffracted X-ray intensity is therefore larger for atoms with larger atomic number (Z).

Neutrons interact directly with the nucleus of the atom, and the contribution to the diffracted intensity depends on each isotope.

It is also often the case that light atoms contribute strongly to the diffracted intensity even in the presence of large Z atoms. The scattering length varies from isotope to isotope rather than linearly with the atomic number.

MD simulation

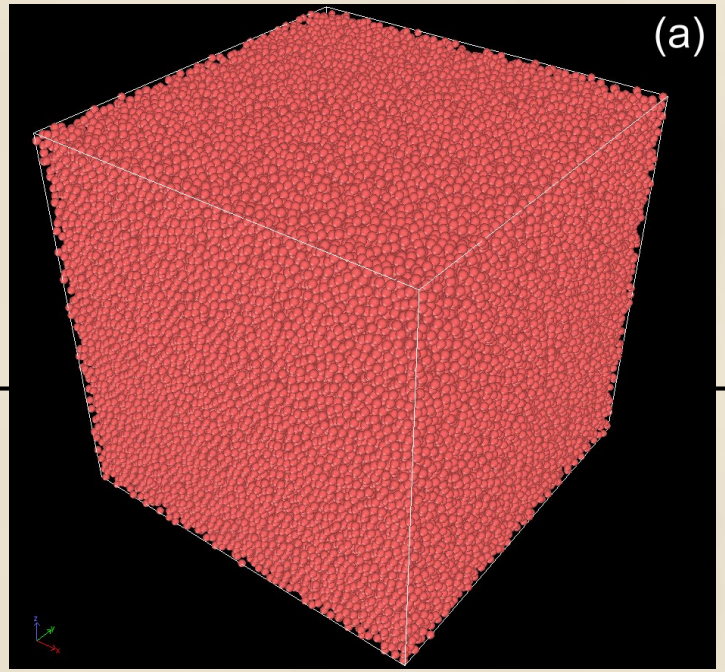

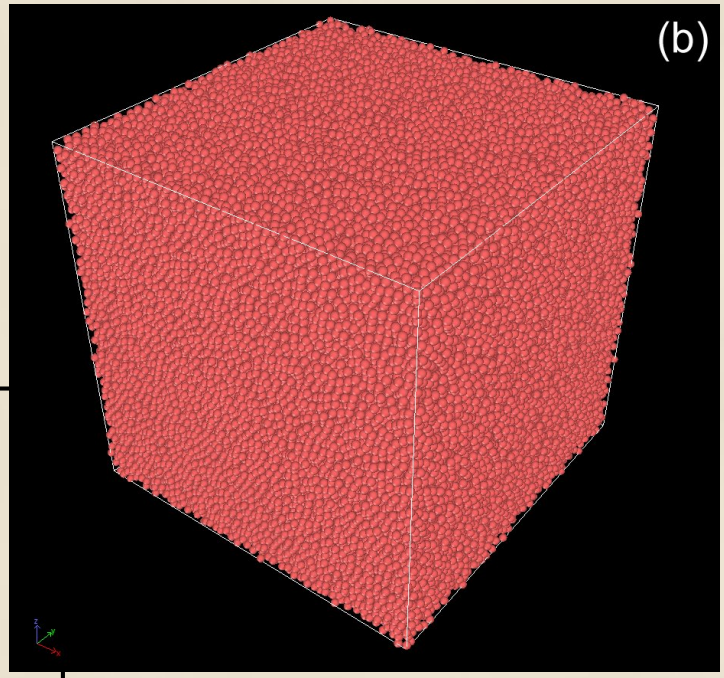

liquid (L) Fe

glass (G)

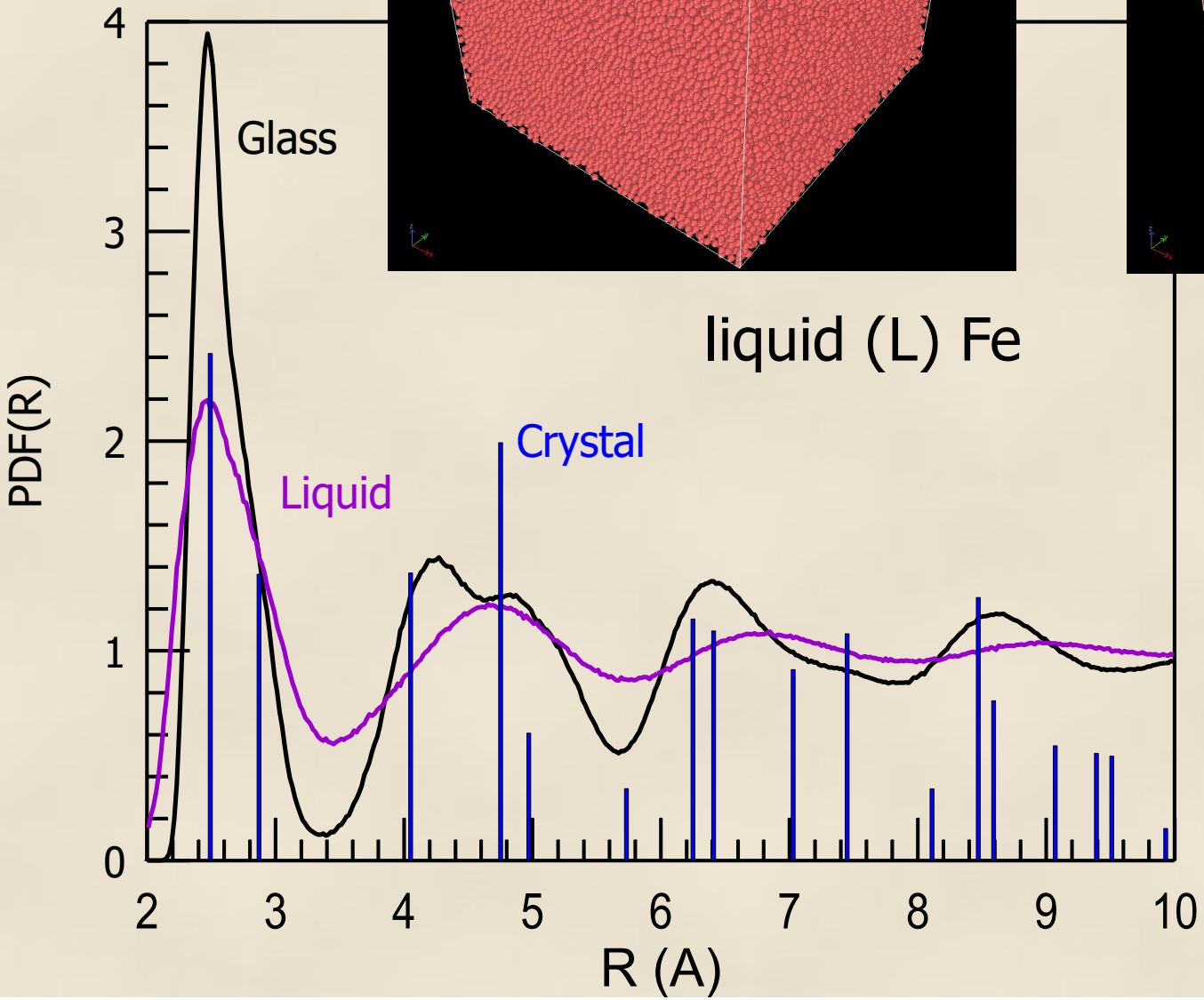

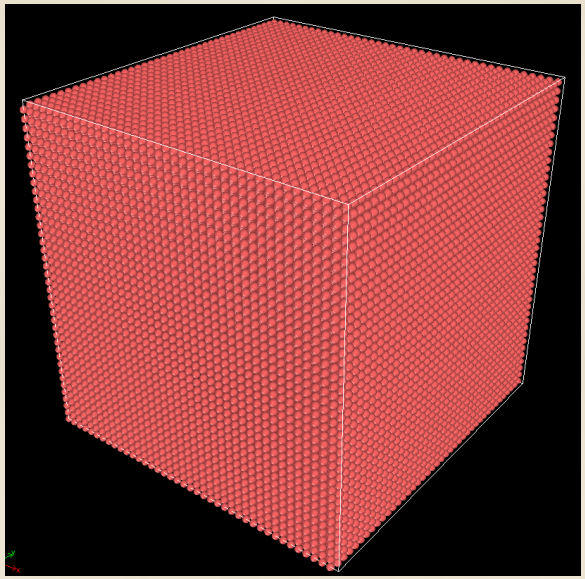

Crystal

Structural changes on cooling

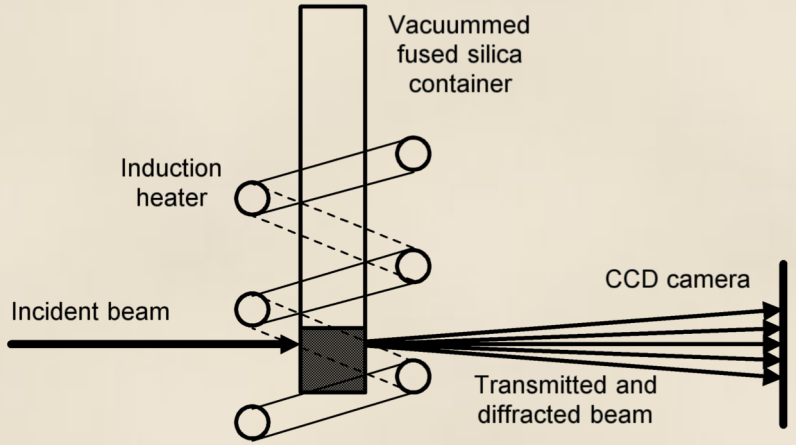

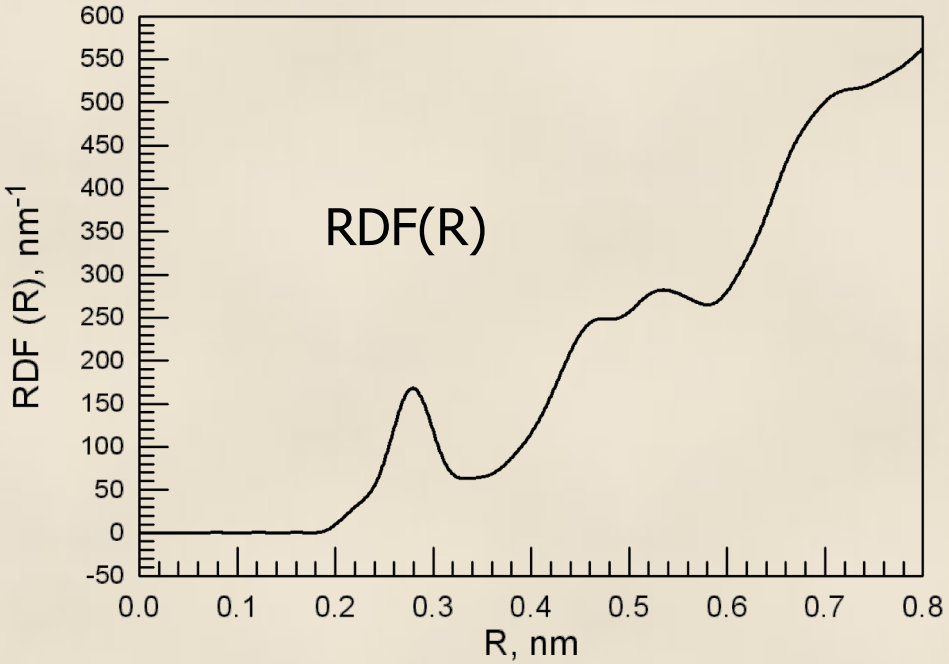

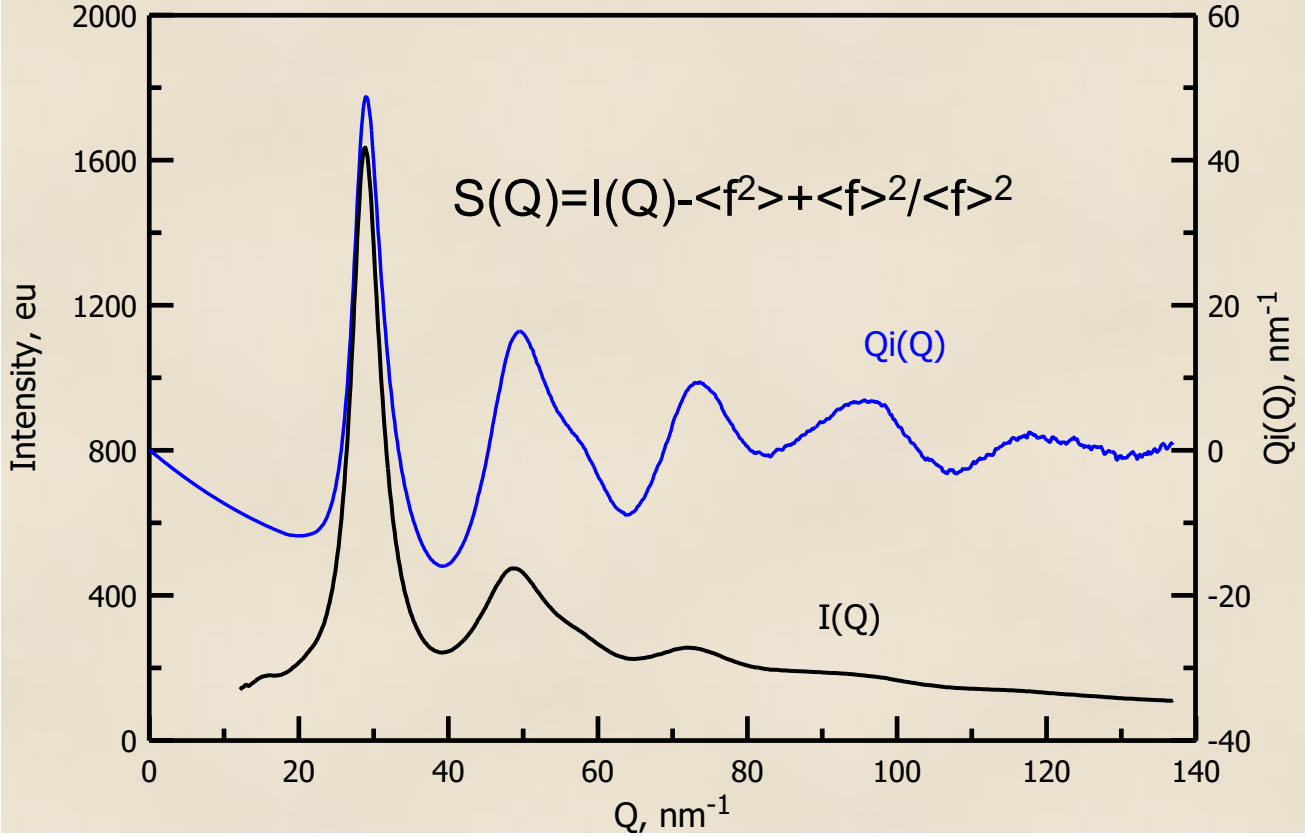

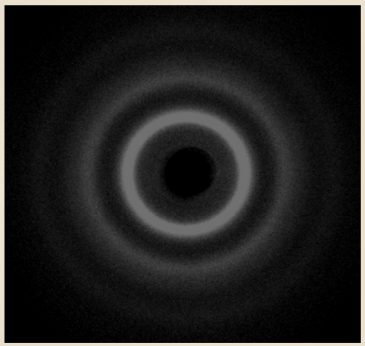

$Pd_{42.5}Cu_{30}Ni_{7.5}P_{20}$

Structural changes in liquid on cooling and heating

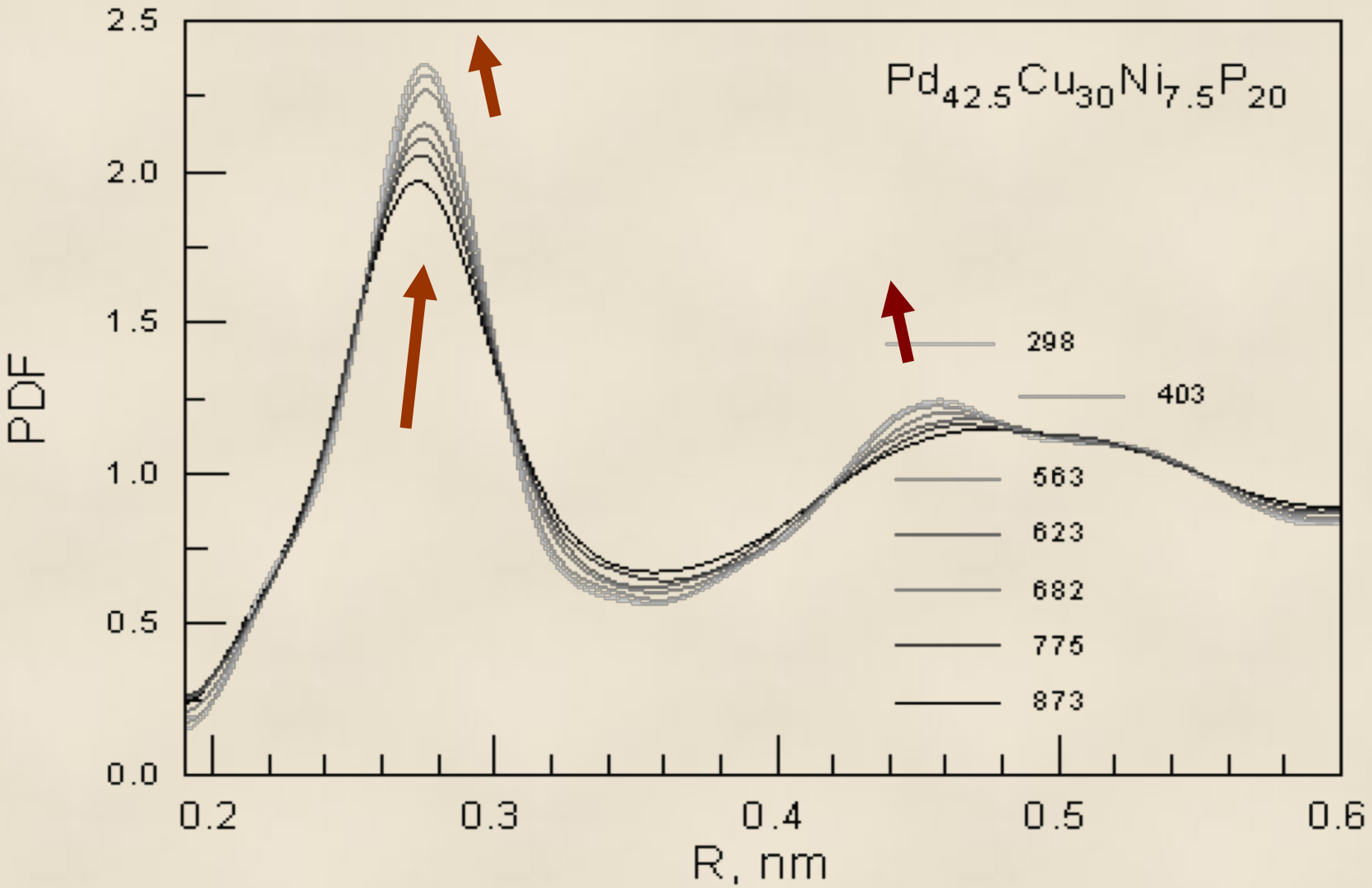

K. Georgarakis, D. V. Louzguine-Luzgin, J. Antonowicz, G. Vaughan, A. R. Yavari, T. Egami and A. Inoue, "Variations in atomic structural features of a supercooled Pd–Ni–Cu–P glass forming liquid during in situ vitrification" Acta Materialia, Vol. 59, N: 2, (2011) pp. 708–716.

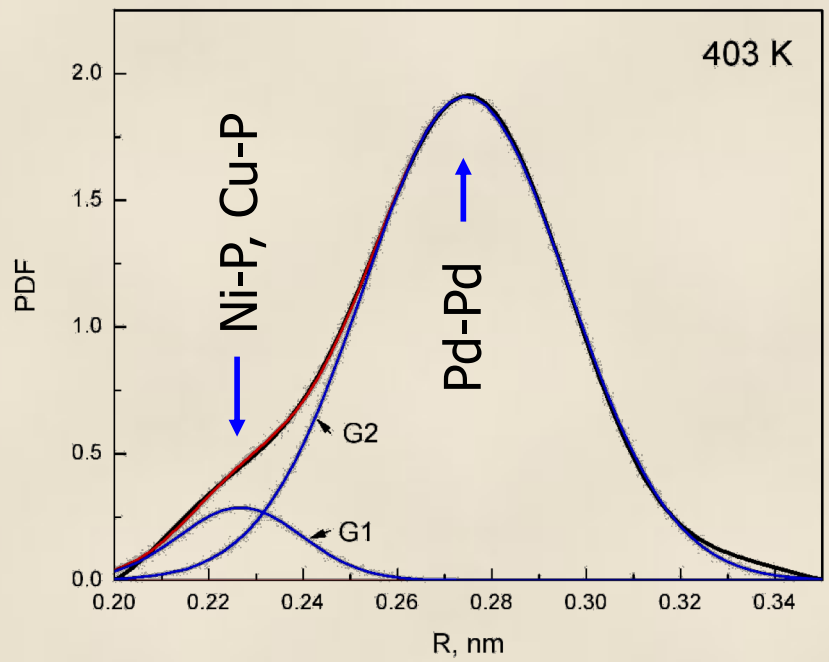
403 K
Ni-P, Cu-P
Pd-Pd
G2
G1
PDF
R, nm

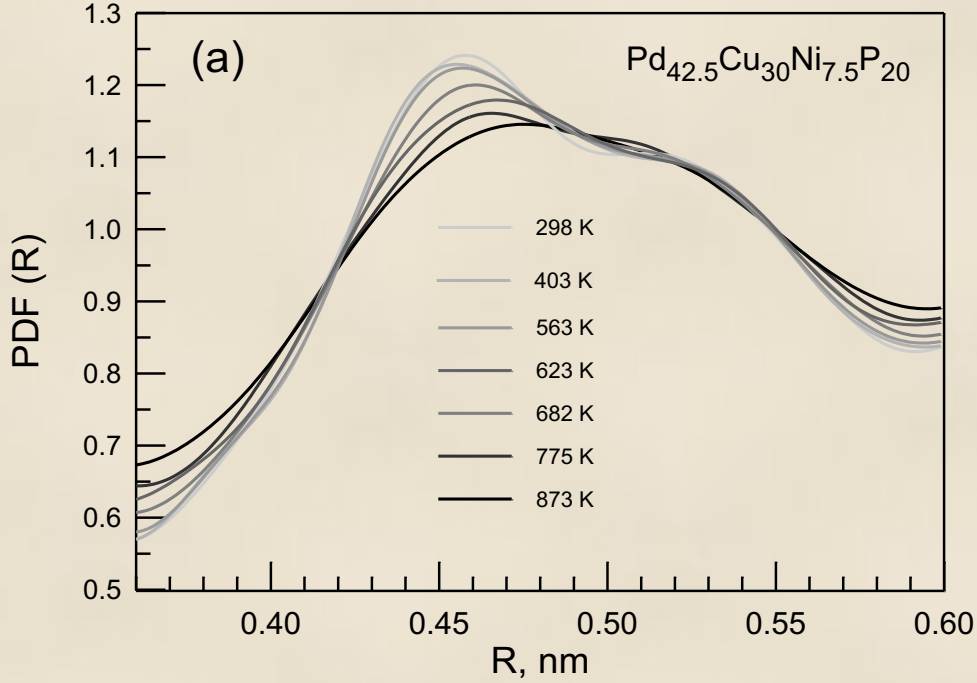
(a)
$Pd_{42.5}Cu_{30}Ni_{7.5}P_{20}$
298 K
403 K
563 K
623 K
682 K
775 K
873 K
PDF (R)
R, nm

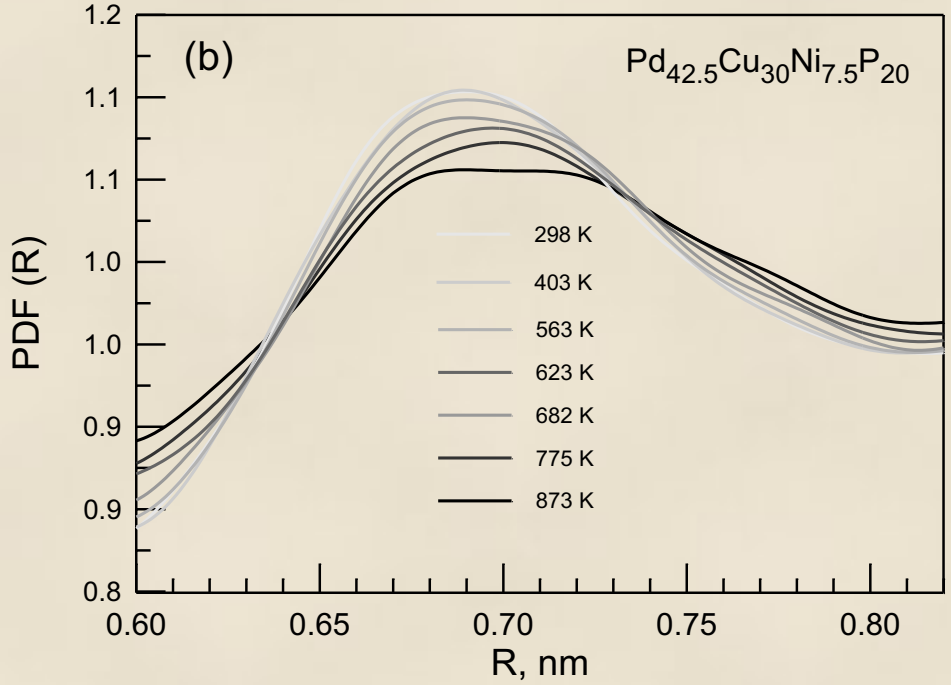
(b)
$Pd_{42.5}Cu_{30}Ni_{7.5}P_{20}$
298 K
403 K
563 K
623 K
682 K
775 K
873 K
PDF (R)
R, nm

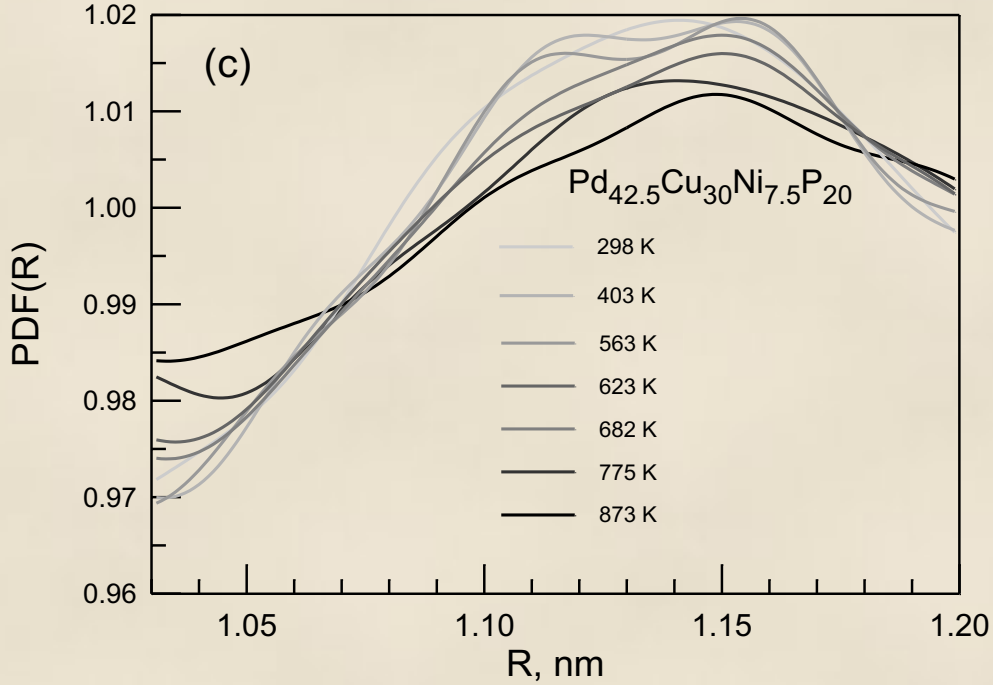
(c)
$Pd_{42.5}Cu_{30}Ni_{7.5}P_{20}$
298 K
403 K
563 K
623 K
682 K
775 K
873 K
PDF(R)
R, nm

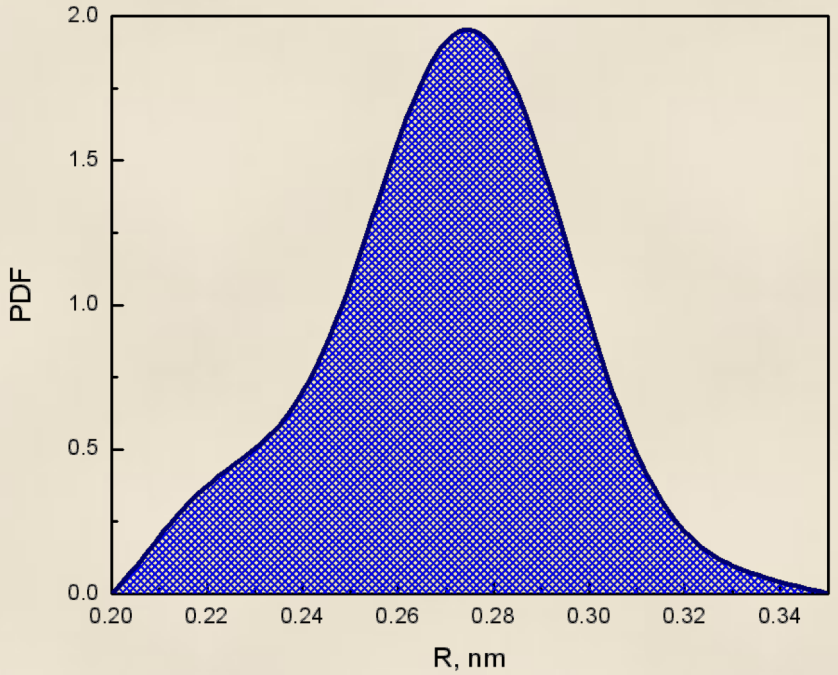
PDF
R, nm
2.0
1.5
1.0
0.5
0.0
0.20
0.22
0.24
0.26
0.28
0.30
0.32
0.34

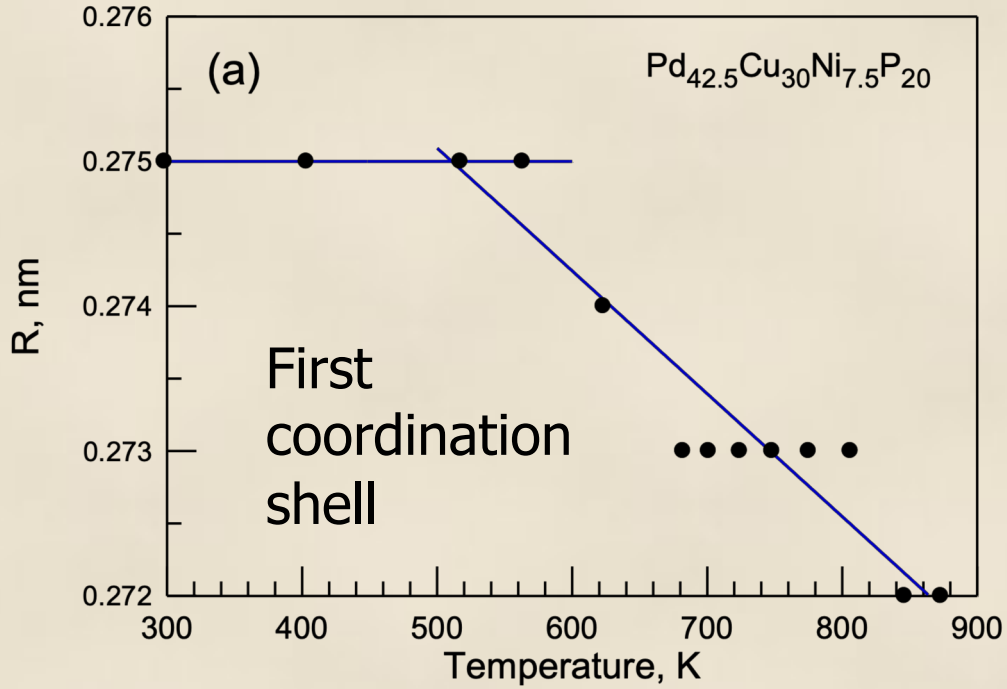
(a)
$Pd_{42.5}Cu_{30}Ni_{7.5}P_{20}$
First coordination shell
R, nm
Temperature, K
0.276
0.275
0.274
0.273
0.272
300
400
500
600
700
800
900

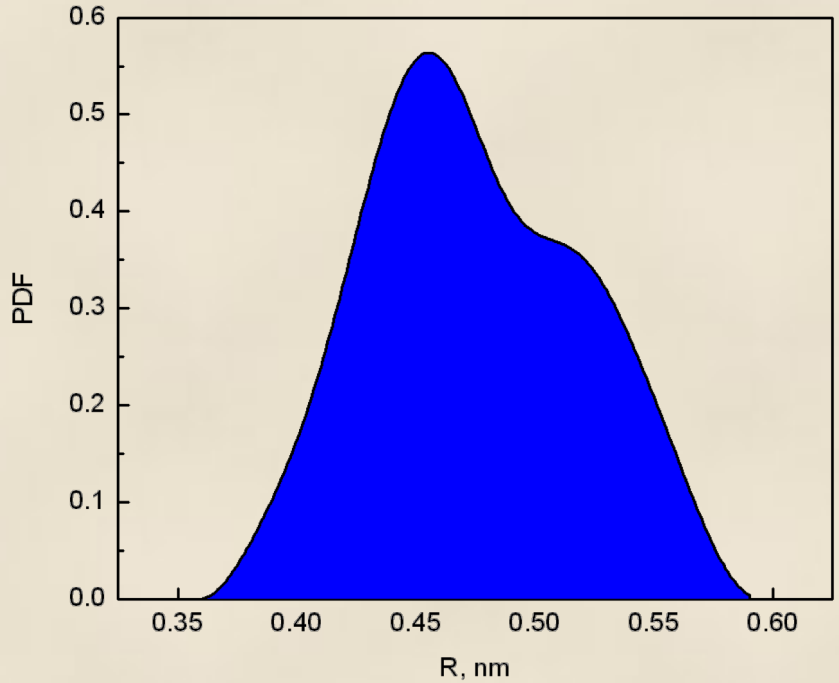
PDF
R, nm
0.6
0.5
0.4
0.3
0.2
0.1
0.0
0.35
0.40
0.45
0.50
0.55
0.60

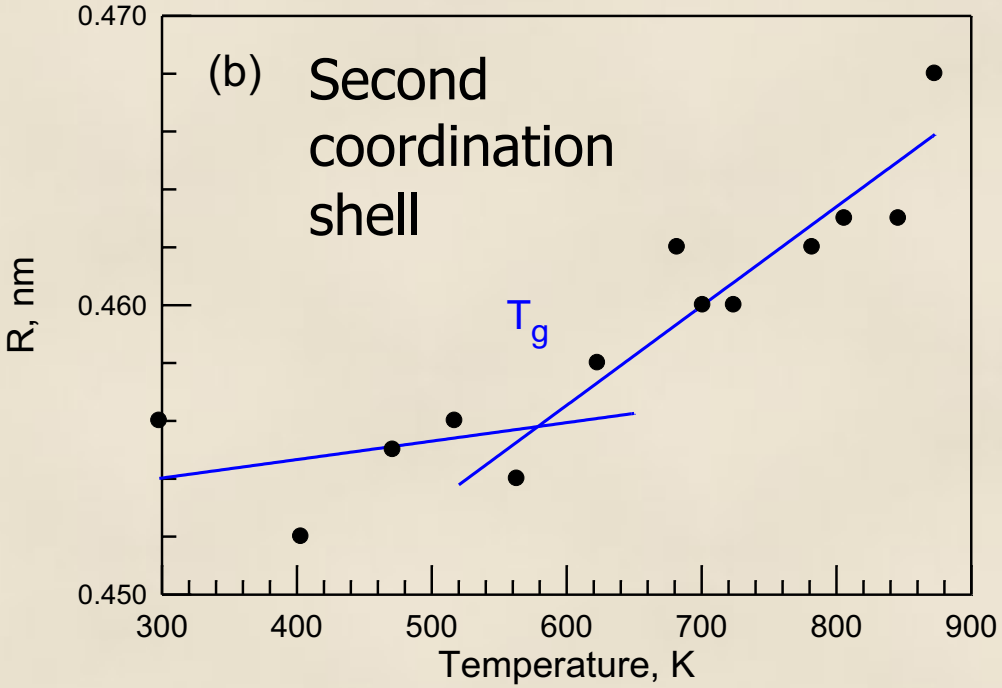
(b)
Second coordination shell
T_g
R, nm
Temperature, K
0.470
0.460
0.450
300
400
500
600
700
800
900

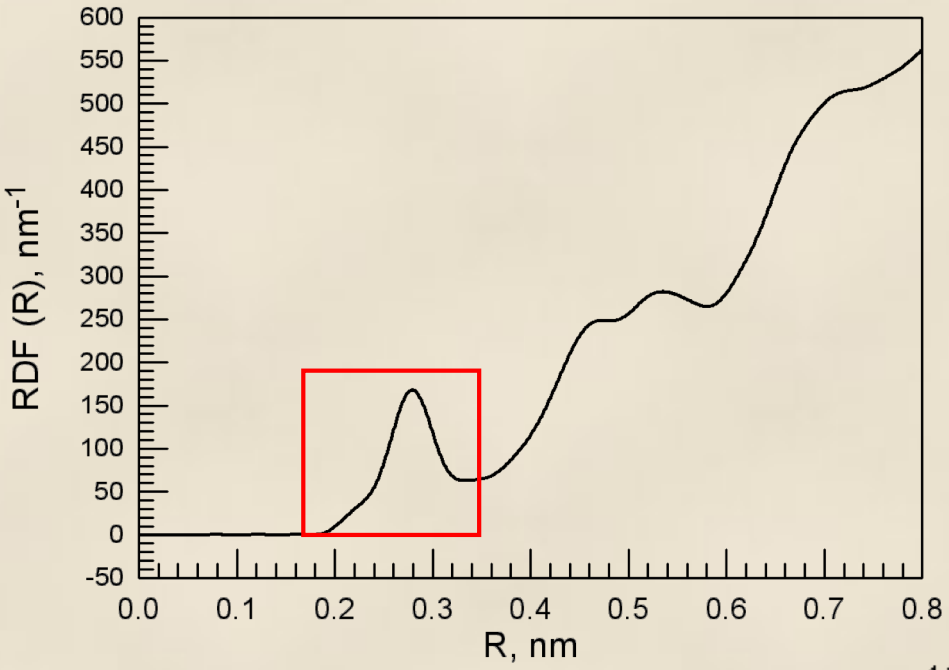

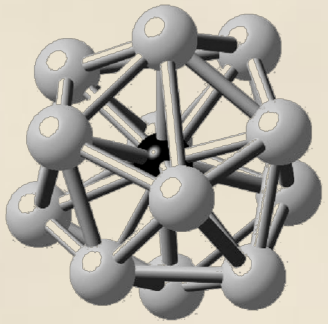

Efficient packing of atoms in clusters and clusters in space

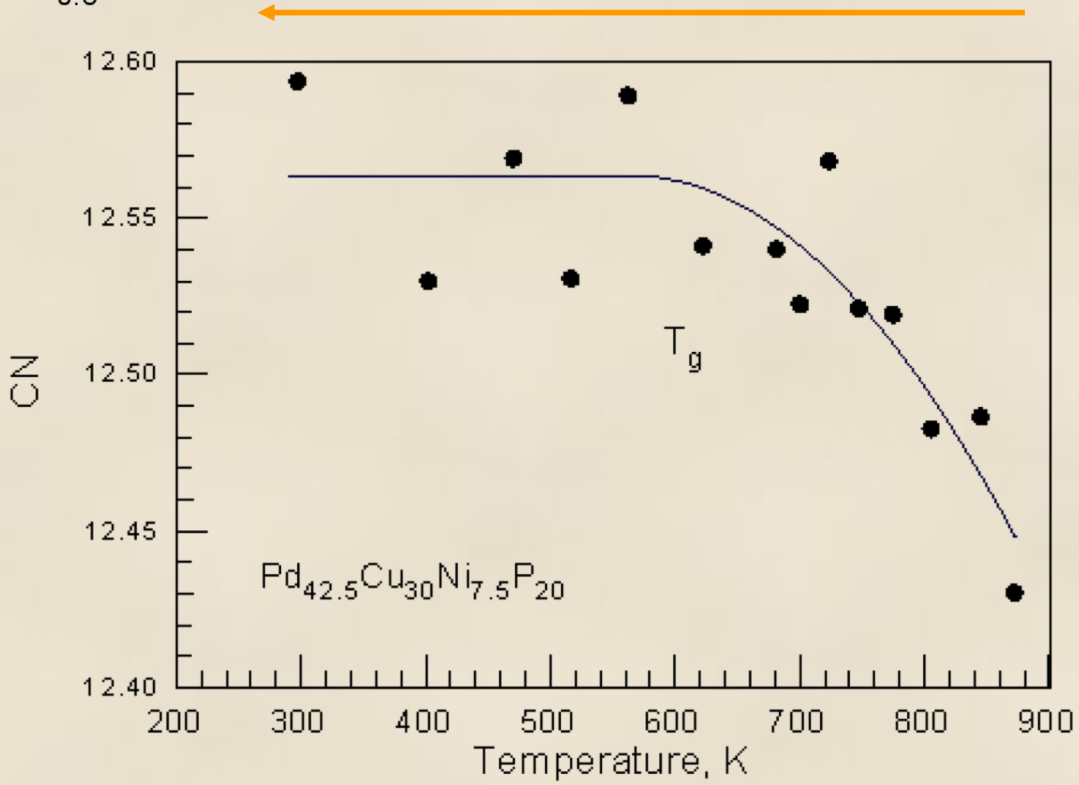

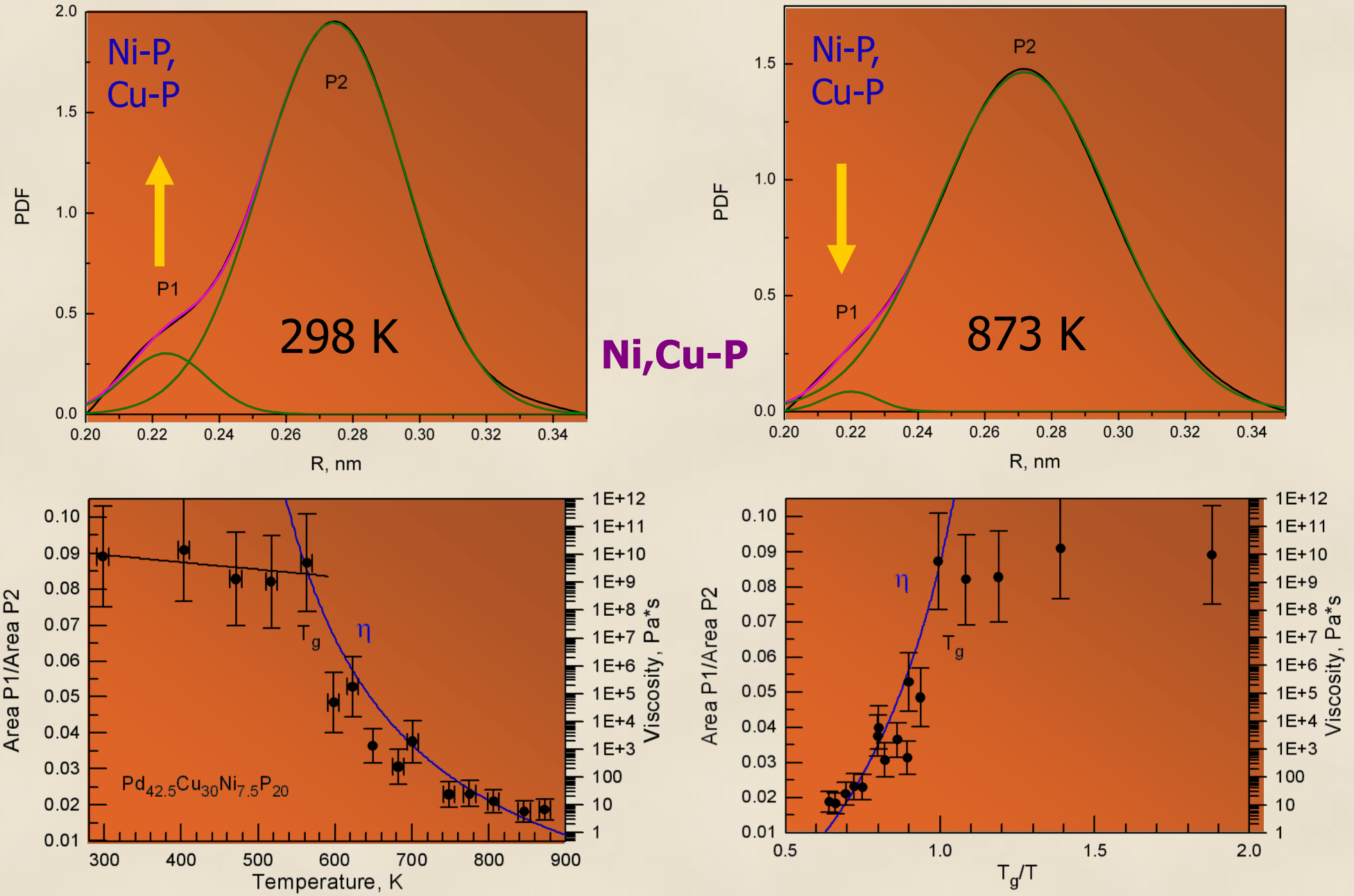

D. V. Louzguine-Luzgin, R. Belosludov, A. R. Yavari, K. Georgarakis, G. Vaughan, Y. Kawazoe, T. Egami, and A. Inoue "Structural basis for supercooled liquid fragility established by synchrotron-radiation method and computer simulation" Journal of Applied Physics, Vol. 110, N:4 (2011) pp. 043519.

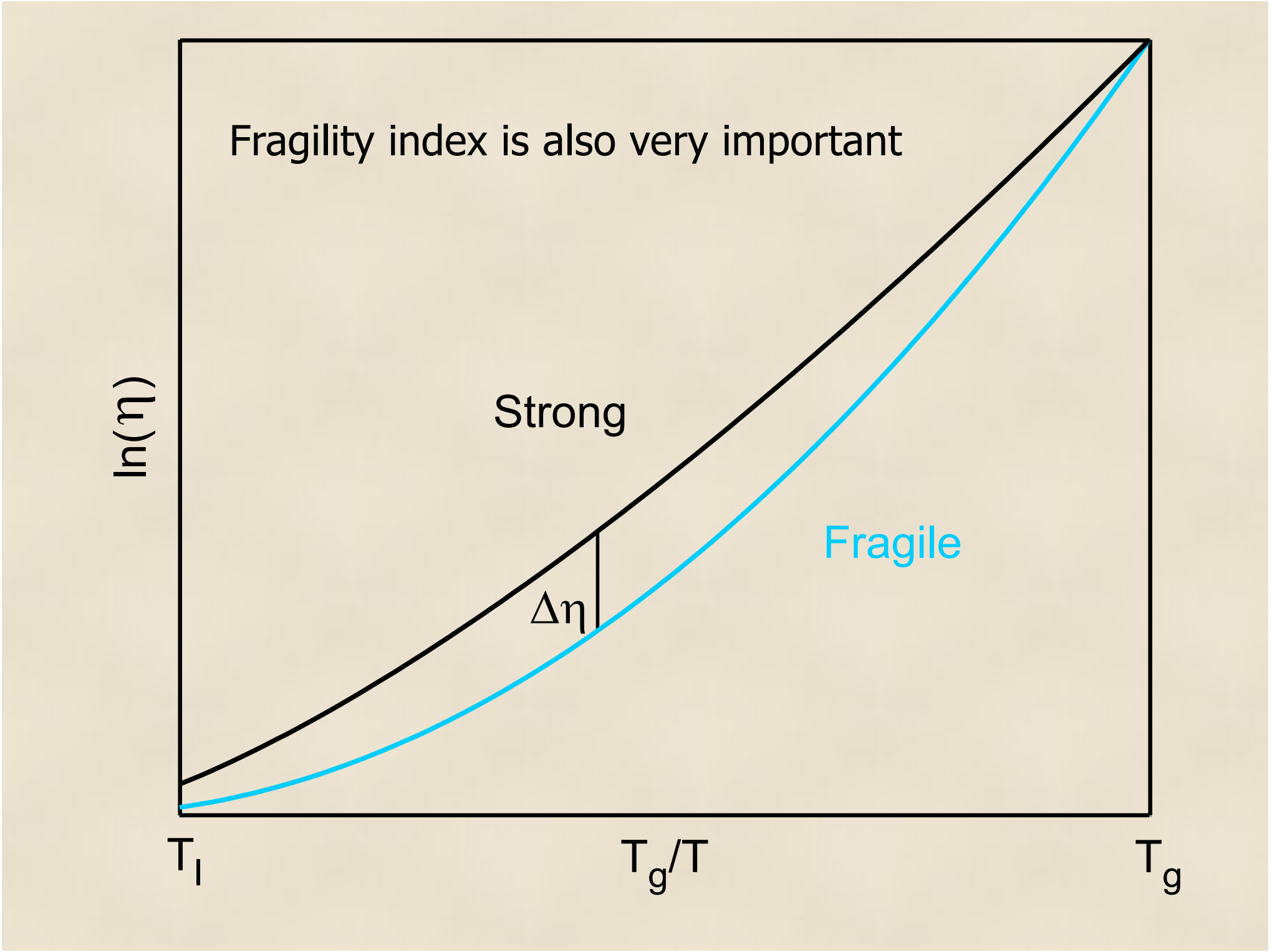
Fragility index is also very important
ln(η)
Strong
Fragile
Δη
T_l
T_g/T
T_g

MD simulation

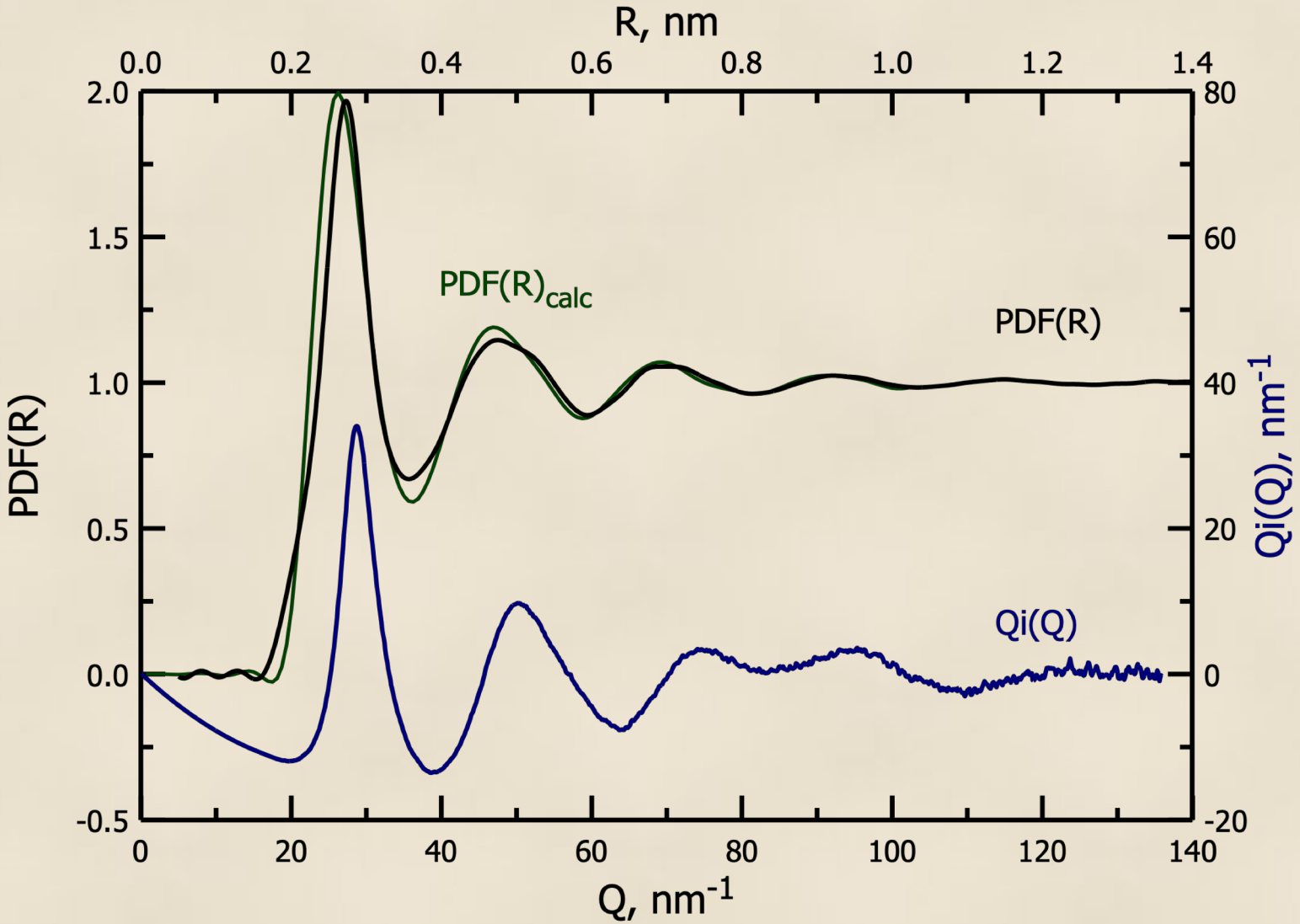

(a)

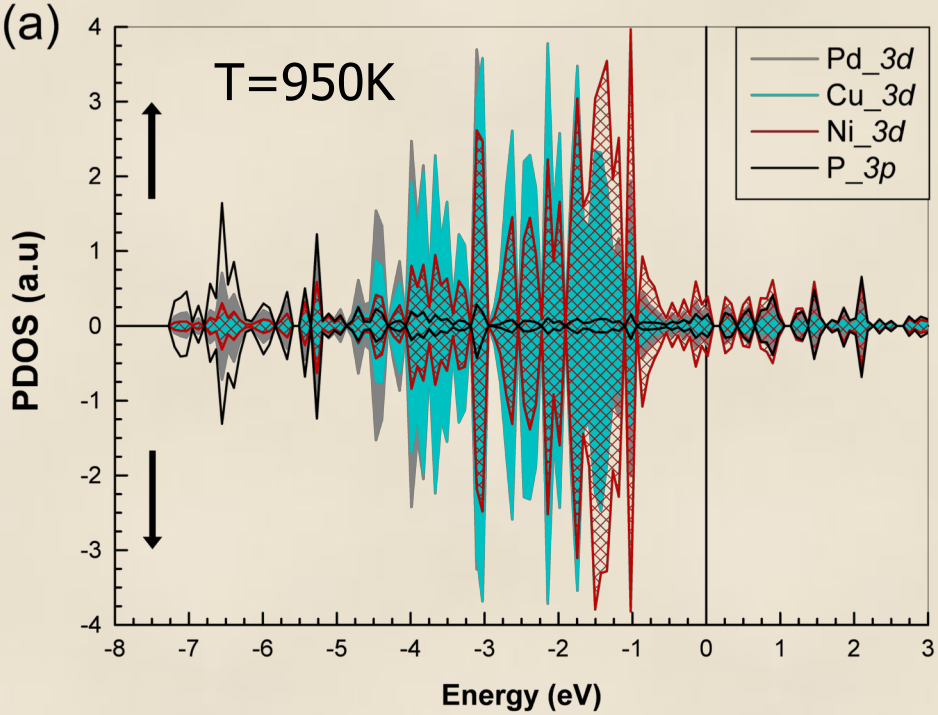

Partial densities of states (PDOS)

In the case of liquid the higher intensity of electron density below the Fermi level corresponds to metal atoms are observed. The significant reduction of peak intensities for metal atoms in this energy region is found during the glass formation. In contrast, the electron density of 3p state of phosphorus atoms increased below Fermi level that indicates the formation of chemical bonds with p-d hybridization between P and metal atoms due to charge transfer from metal to the phosphorous.

PDOS for the spin-up (↑) and spin-down (↓) *3d* electrons of the Pd (gray), Cu (blue), Ni (red) and *3p* electron P (black) atoms, at T= 950K (a) and at T= 550K (b) respectively. The Fermi level (vertical line) has been chosen as zero energy.

(b)

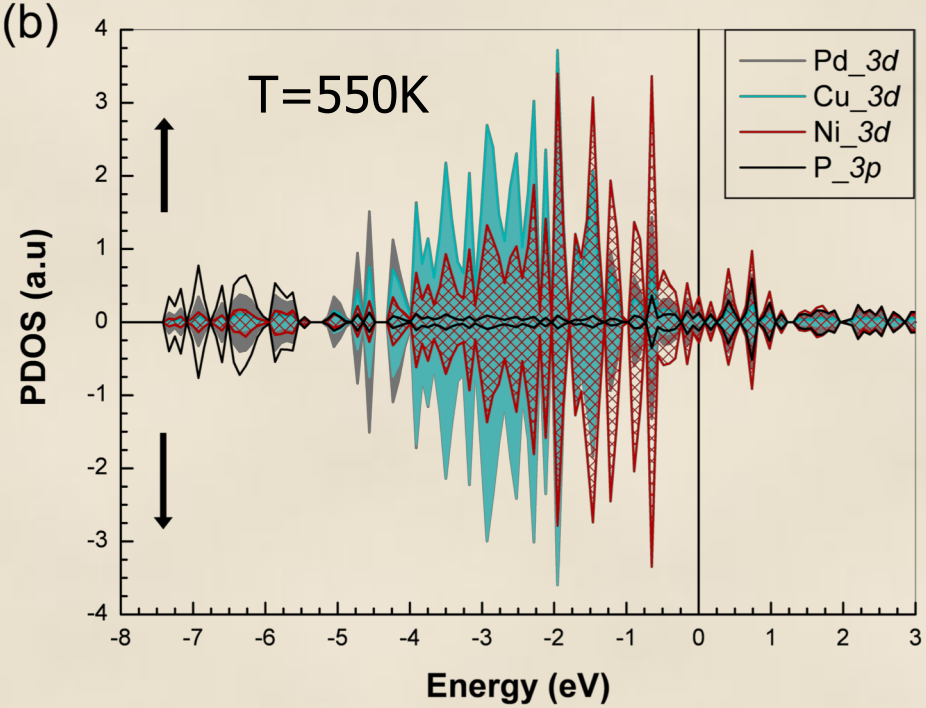

On supercooling, the relative integrated intensity of a low-R subpeak (P1) of the 1st coordination shell in the PDF becomes stronger on cooling from the melt to T_g.

Such an increase in the sub-peak intensity indicates formation of the atomic clusters with P at the center and Ni and Cu at the nearest neighbor that are bonded to P covalently during supercooling of the melt.

These bonds determine fragility of the melt.

More detailed structural information can be obtained by using anomalous X-ray scattering (AXS) [i], the X-ray absorption fine structure (XAFS) [ii], including the extended X-ray absorption fine structure (EXAFS) [iii, iv] and X-ray absorption near edge structure (XANES) [v] when environmental RDFs for certain atomic pairs can be obtained.

[i] D. V. Louzguine, M. Saito, Y. Waseda and A. Inoue, Structural study of amorphous $Ge_{50}Al_{40}Cr_{10}$ alloy, Journal of the Physical Society of Japan, 68 (1999) 2298-2303.

[ii] J. Antonowicz, A. Pietnoczka, K. Pękała, J. Latuch, G.A. Evangelakis, Local atomic order, electronic structure and electron transport properties of Cu-Zr metallic glasses, J. Appl. Phys. 115 (2014) 203714.

[iii] W.K. Luo, E. Ma, EXAFS measurements and reverse Monte Carlo modeling of atomic structure in amorphous $Ni_{80}P_{20}$ alloys, J. Non-Cryst Solids, 354 (2008) 945–955.

[iv] J. Antonowicz, A. Pietnoczka, W. Zalewski, R. Bacewicz, M. Stoica, K. Georgarakis, A.R. Yavari, Local atomic structure of Zr–Cu and Zr–Cu–Al amorphous alloys investigated by EXAFS method, J. Alloys Compd. 509S (2011) S34.

[v] A. L. Ankudinov, B. Ravel, J. J. Rehr, and S. D.Conradson, Real-space multiple-scattering calculation and interpretation of X-ray-absorption near-edge structure, Phys. Rev. B 58 (1998) 7565–7576.

Anomalous X-ray scattering

D. V. Louzguine, M. Saito, Y. Waseda and A. Inoue "Structural study of amorphous $Ge_{50}Al_{40}Cr_{10}$ alloy", Journal of the Physical Society of Japan, Vol. 68, N: 7 (1999) pp. 2298-2303

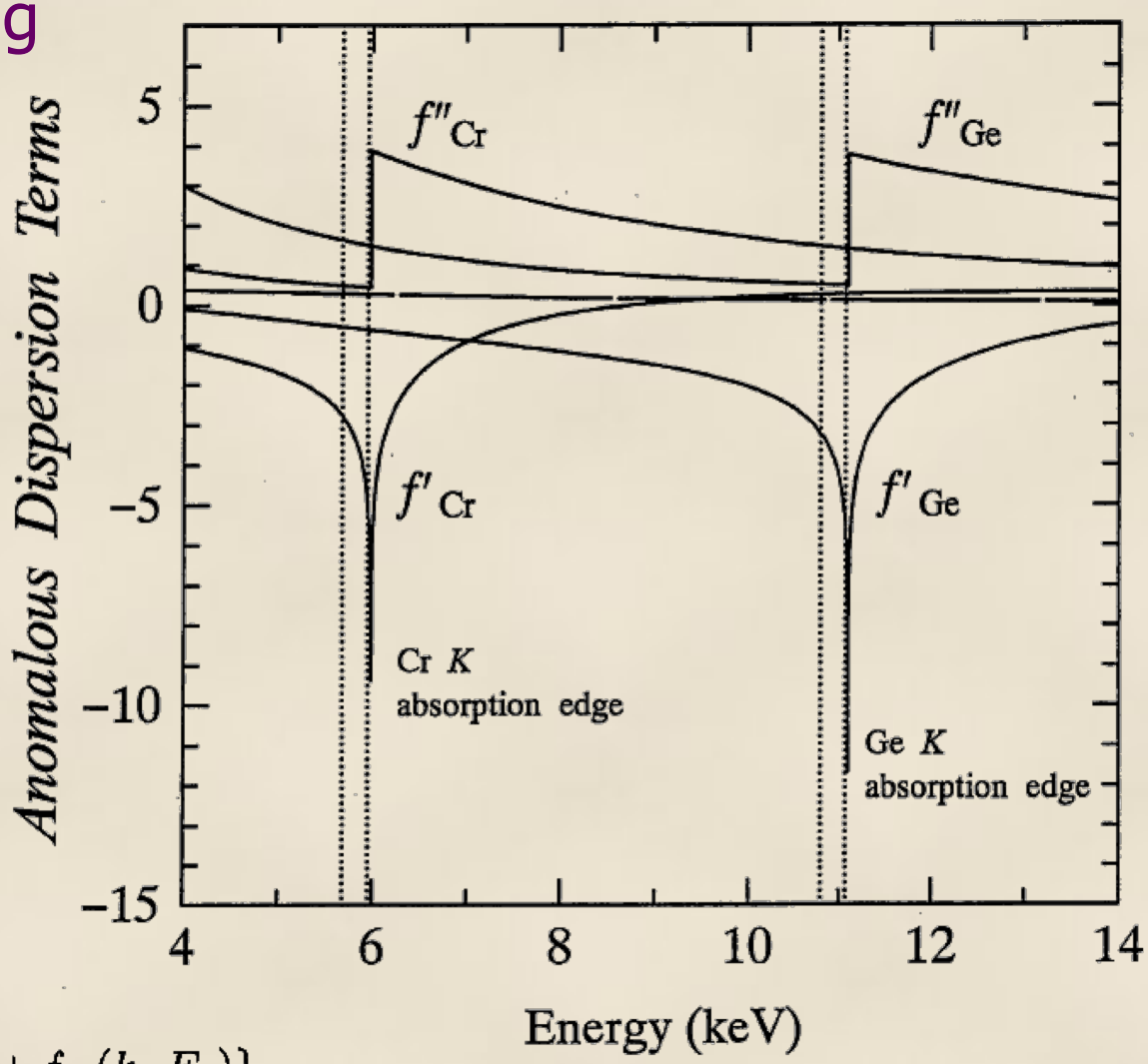

$$W(k, E_1, E_2) = \sum_{m=1}^{3} c_m \mathcal{R}\{f_m(k, E_1) + f_m(k, E_2)\}$$

$$\Delta i_{\mathrm{Ge}}(k, E_1, E_2) \cong \frac{\{I_{\mathrm{obs}}(k, E_1) - \langle f^2(k, E_1)\rangle\} - \{I_{\mathrm{obs}}(k, E_2) - \langle f^2(k, E_2)\rangle\}}{c_{\mathrm{Ge}}\{f'_{\mathrm{Ge}}(E_1) - f'_{\mathrm{Ge}}(E_2)\}W(k, E_1, E_2)}$$

$$= \sum_{m=1}^{3} \frac{c_m \mathcal{R}\{j_m(k, E_1) + j_m(k, E_2)\}}{W(k, E_1, E_2)}\{a_{\mathrm{Gem}}(k) - 1\},$$

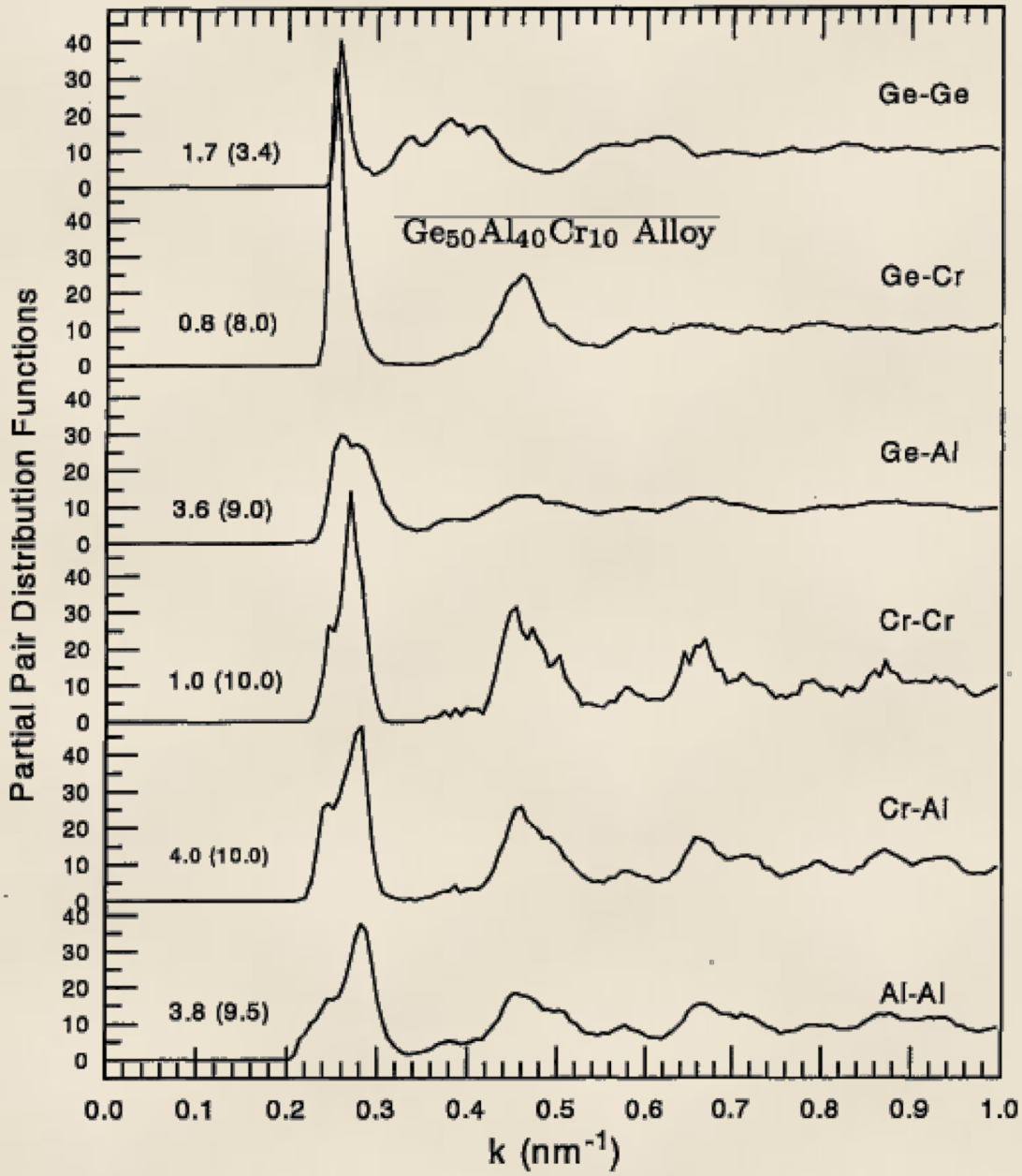

Fig. 7. Partial pair distribution functions.

D. V. Louzguine, M. Saito, Y. Waseda and A. Inoue “Structural study of amorphous $Ge_{50}Al_{40}Cr_{10}$ alloy”, Journal of the Physical Society of Japan, Vol. 68, (1999) 2298-2303

High-resolution TEM

Crystal (cF96 Ti_2Ni^{ss})

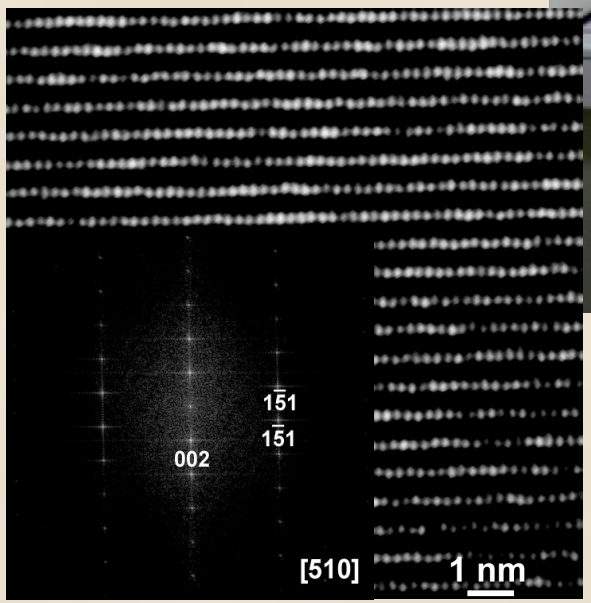

Amorphous/Glass

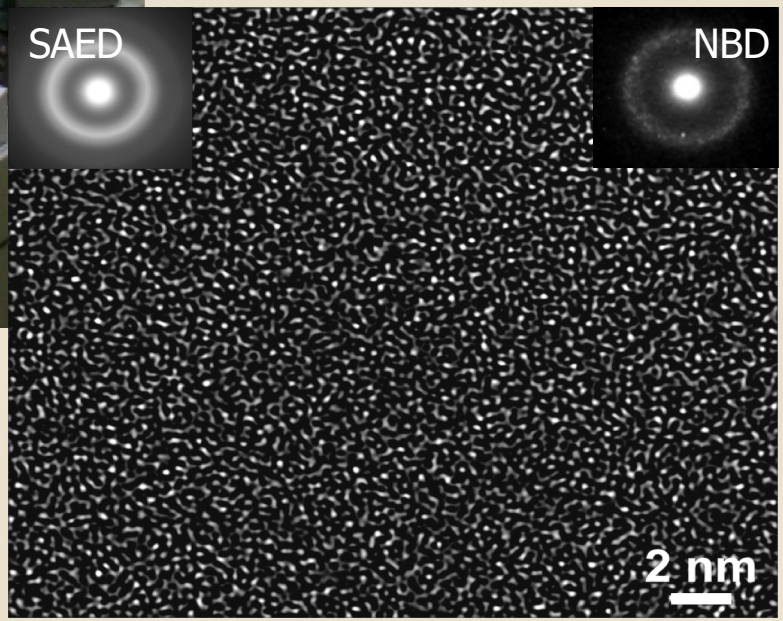

High-resolution transmission electron microscopy TEM

Mechanical Properties

Some BMGs: High Specific Strength (σ/ρ)

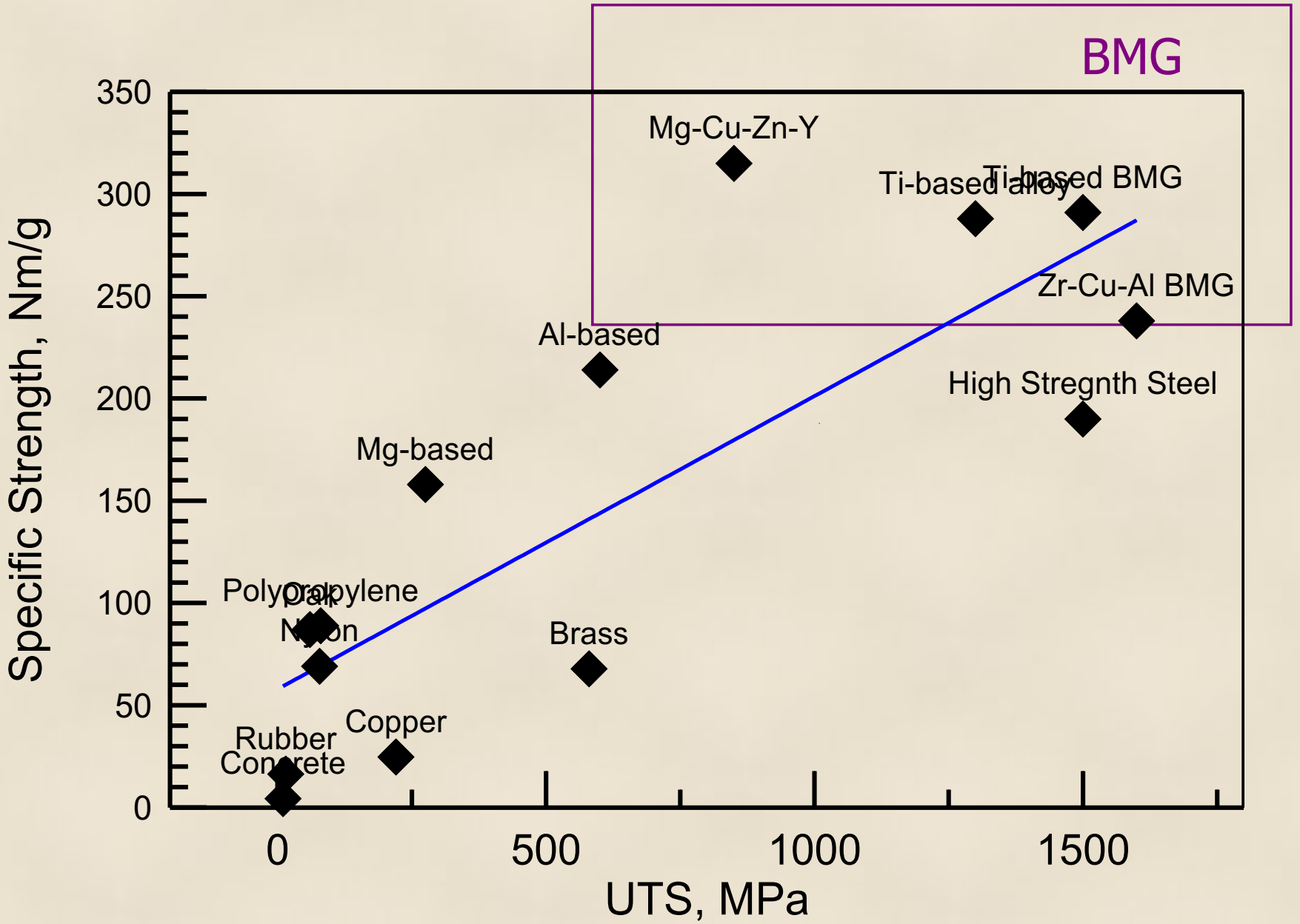

Surface oxides on Cu-Zr-Al BMG D.V. Louzguine-Luzgin, C. L. Chen, L. Y. Lin, Z. C. Wang, S.V. Ketov, M. J. Miyama, A. S. Trifonov, A. V. Lubenchenko, Y. Ikuhara, **Acta Materialia 97 (2015) 282–290**

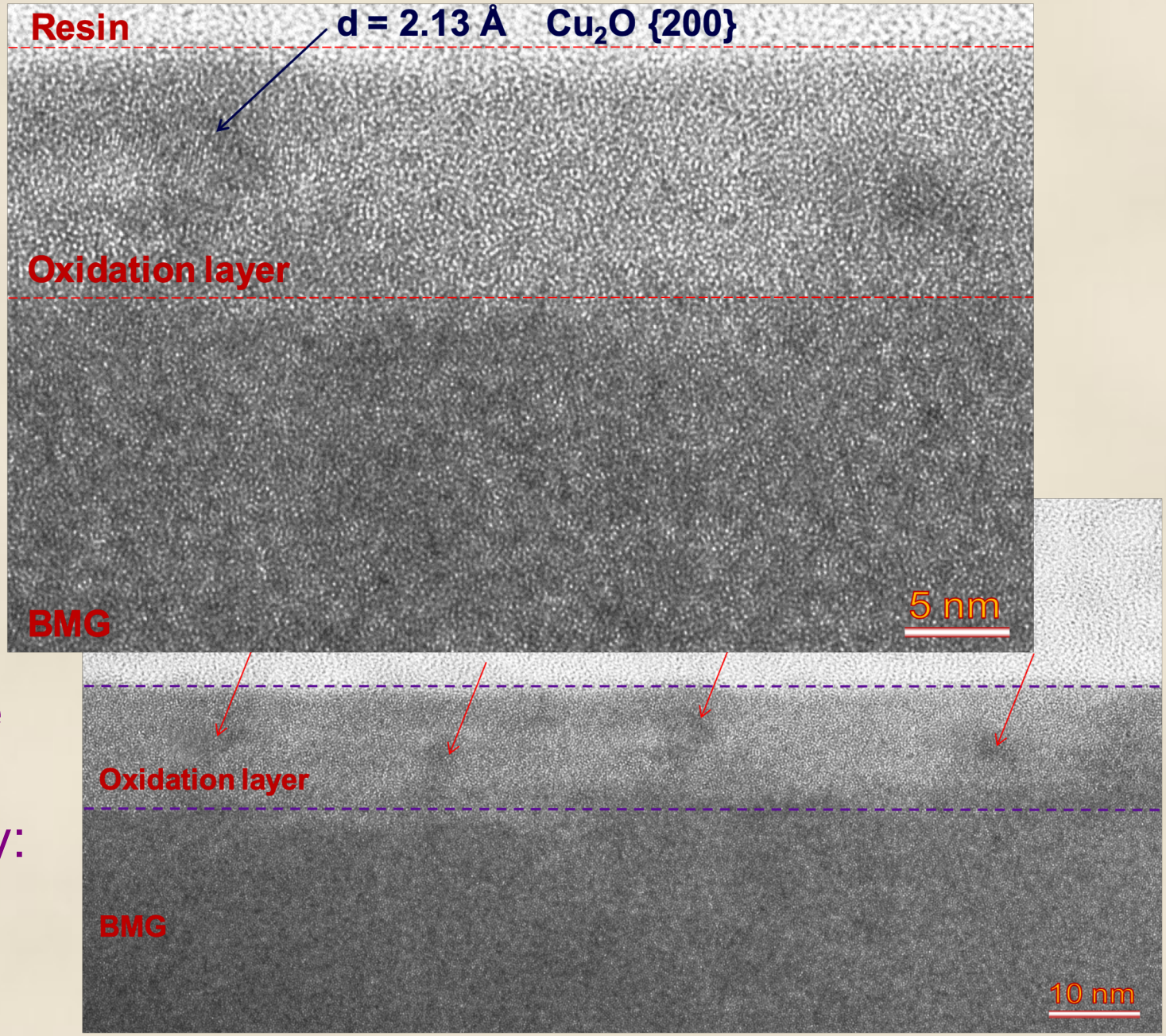

Typical simple $Cu_{47}Zr_{45}Al_8$ BMG alloy: HRTEM images

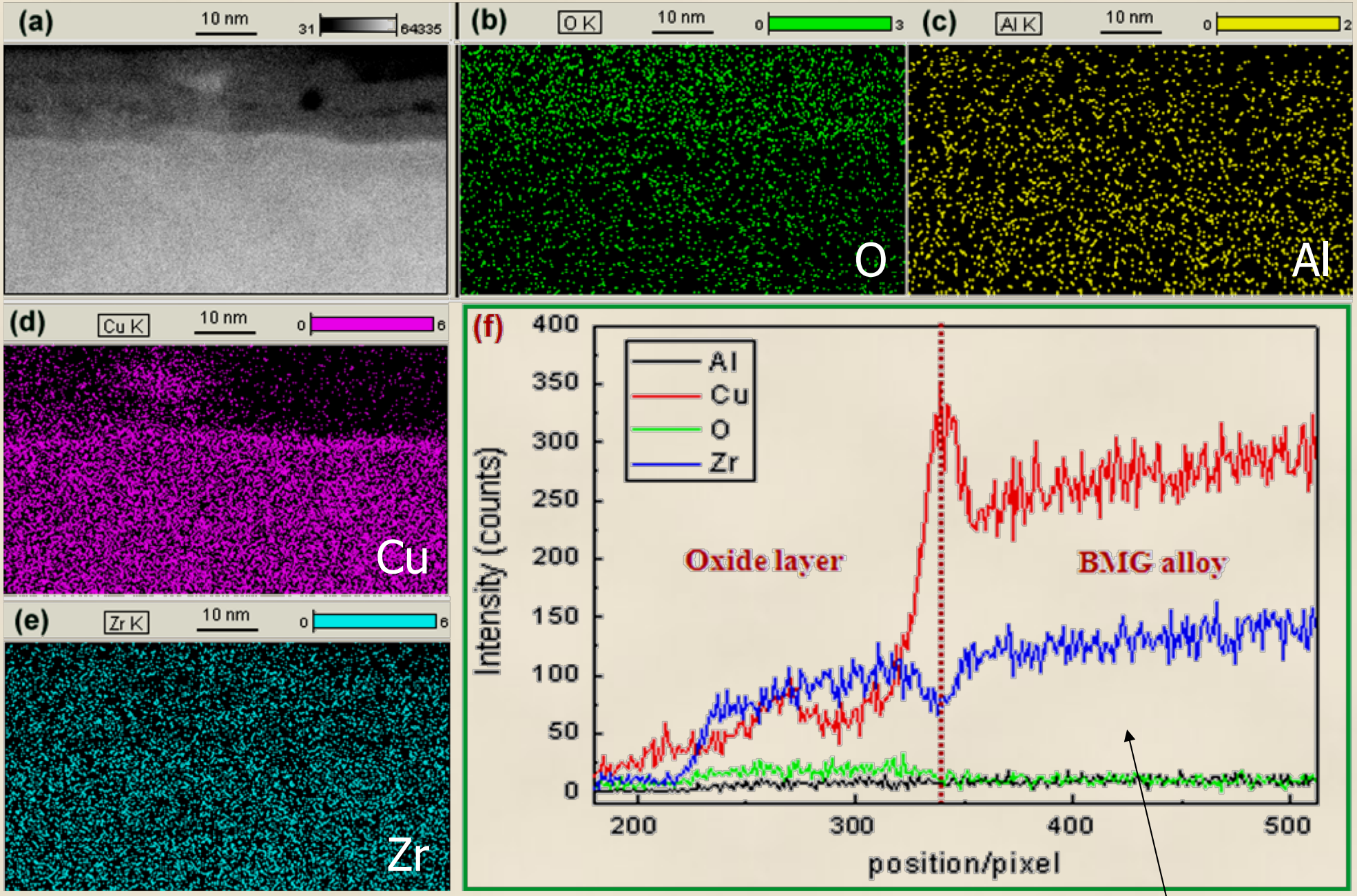

EDX 500 frames with the frame exposure time of 15 s + integrated profile

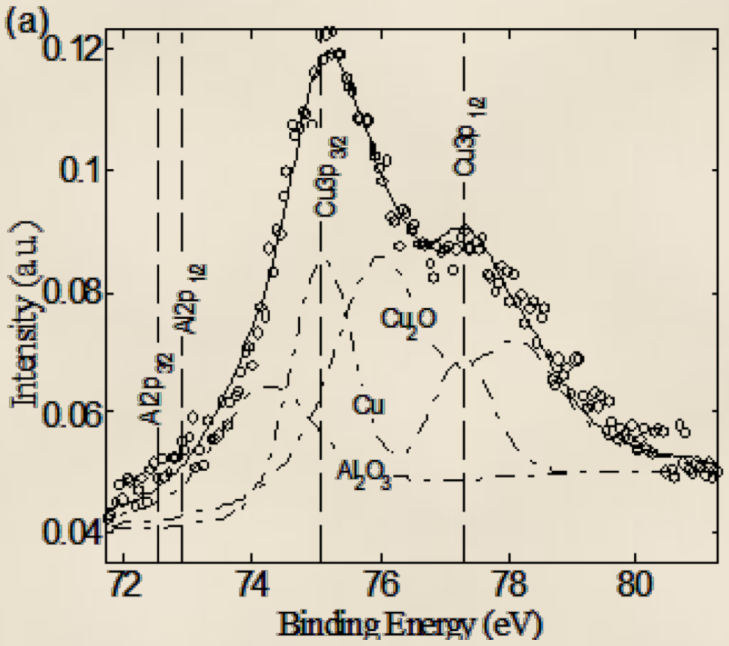

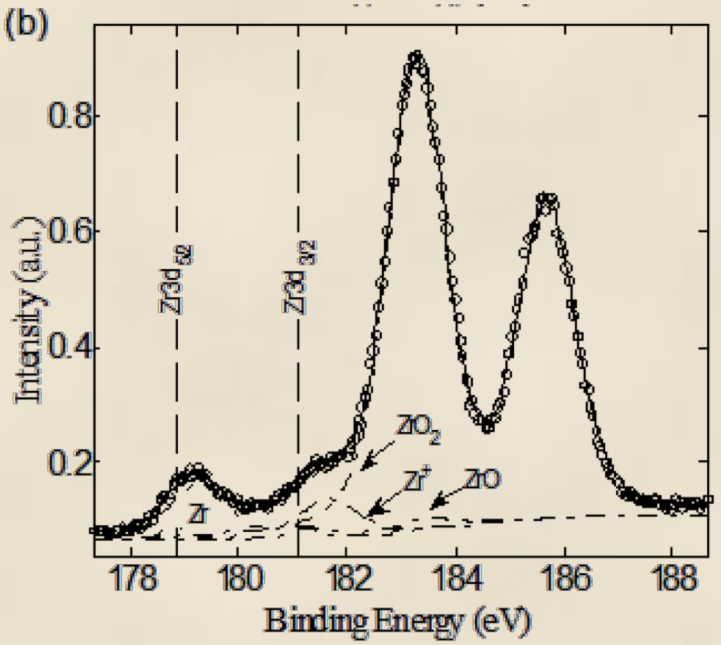

XPS data: increase in Zr content in the oxide, its slow diffusion

	2 hours			10 days			50 days		
	C^t, %		C^p, %	C^t, %		C^p, %	C^t, %		C^p, %
Al	22	Al	0	20	Al	0	12 ↓	Al	0
		Al_2O_3	100		Al_2O_3	100		Al_2O_3	100
Cu	27	Cu	44	22	Cu	38	23	Cu	50
		Cu_2O	56		Cu_2O	62		Cu_2O	50
Zr	51	Zr	3	58	Zr	1	65 ↑	Zr	0
		ZrO_2	77		ZrO_2 ↑	87		ZrO_2	87
		ZrO	4		ZrO	2		ZrO	3
		Zr^+	16		Zr^+	10		Zr^+	10

Z. Wang, S.V. Ketov, C.L. Chen, Y. Shen, Y. Ikuhara, A.A. Tsarkov, D.V. Louzguine-Luzgin, J.H. Perepezko, "Nucleation and thermal stability of an icosahedral nanophase during the early crystallization stage in Zr-Co-Cu-Al metallic glasses", Acta Materialia, 132, (2017), 298-306.

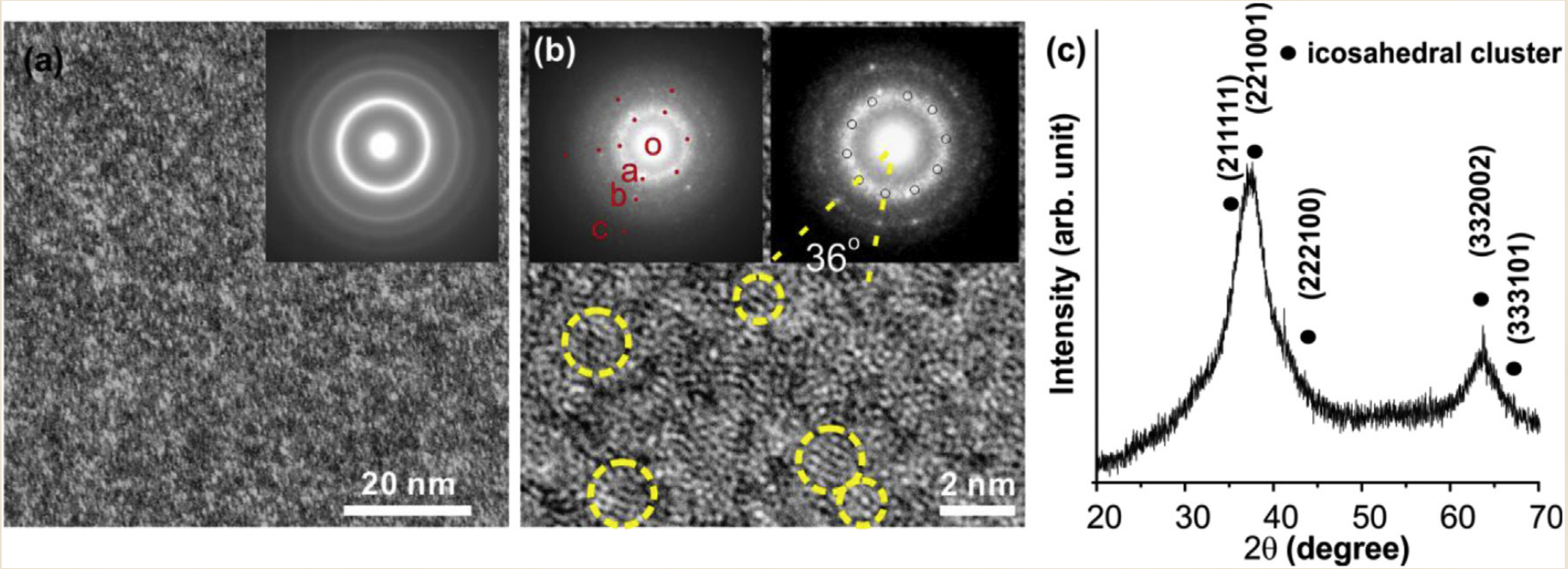

IFE 14 mJ/m^2, ultra-high nucleation density of 6.5*10^{24} m^3 and a size of ~1-2 nm

(a) Dark-field TEM image, (b) HRTEM image of $Zr_{60}Co_{30}Al_{10}$ alloy heated to 823 K, the insert in (a) are the corresponding selected-area electron diffraction pattern; the inserts in (b) are the selected-area electron diffraction patterns. (c) XRD pattern of $Zr_{60}Co_{30}Al_{10}$ alloy heated to 823 K.

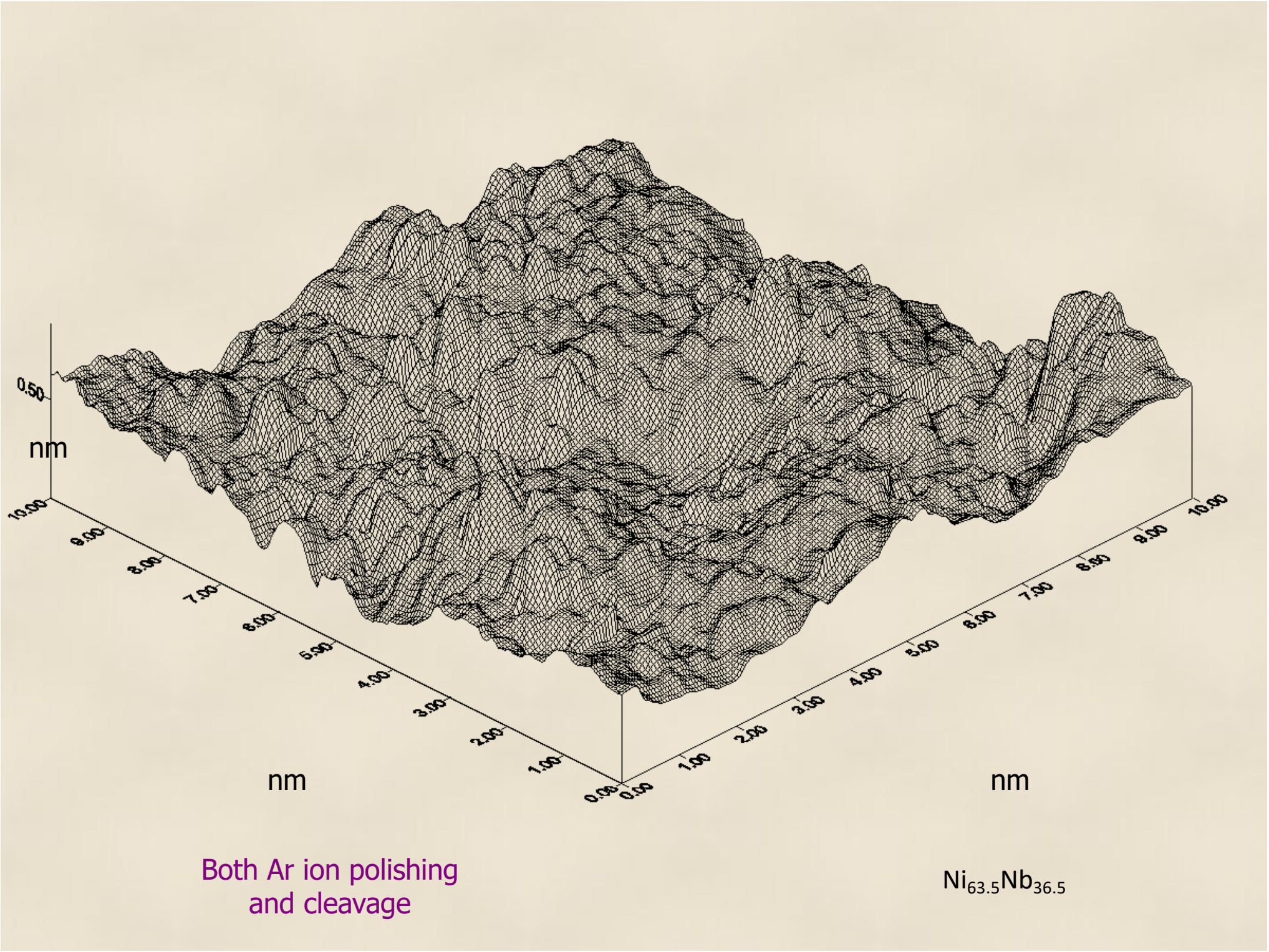

Both Ar ion polishing and cleavage

$Ni_{63.5}Nb_{36.5}$

Cryogenic rejuvenation

S. V. Ketov, Y. H. Sun, S. Nachum, Z. Lu, A. Checchi, A. R. Beraldin, H. Y. Bai, W. H. Wang, D. V. Louzguine-Luzgin, M. A. Carpenter and A. L. Greer, "Rejuvenation of metallic glasses by non-affine thermal strain" **Nature, 524, (2015) 200–203**

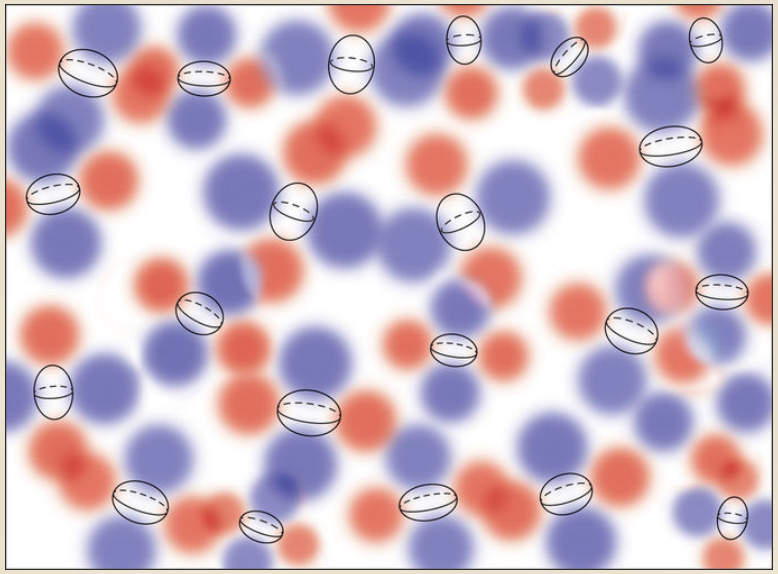

Heterogeneous thermal expansion coefficient: soft and hard zones

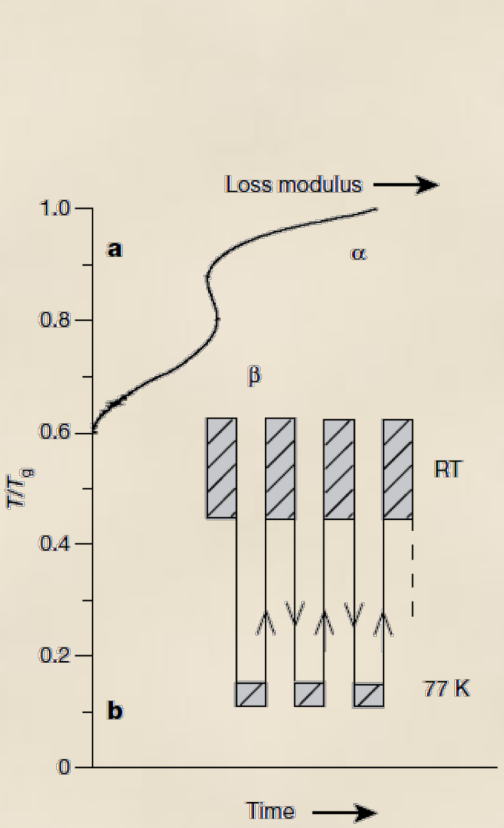

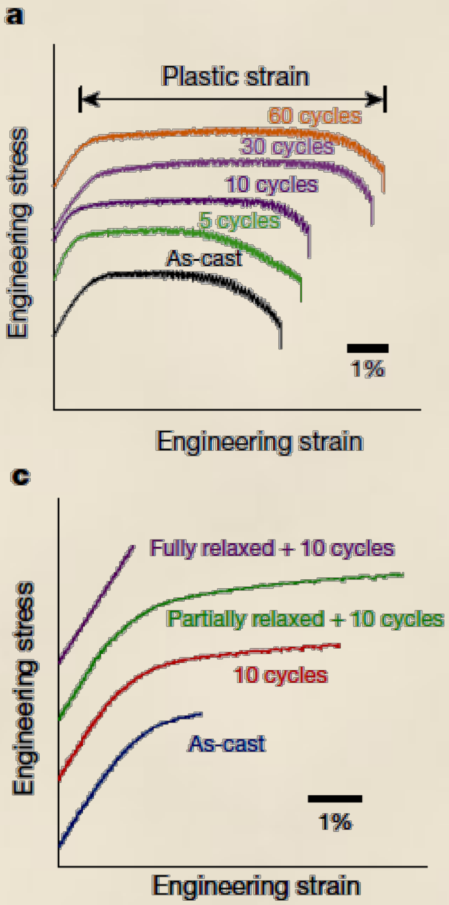

Figure 1 | Thermal cycling of metallic glasses.

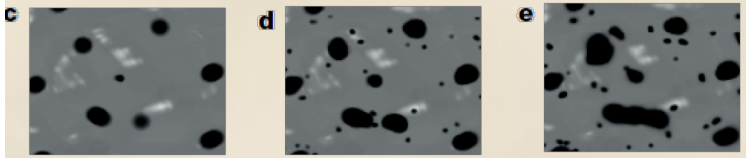

Schematic depictions of the degree of heterogeneity in a metallic glass

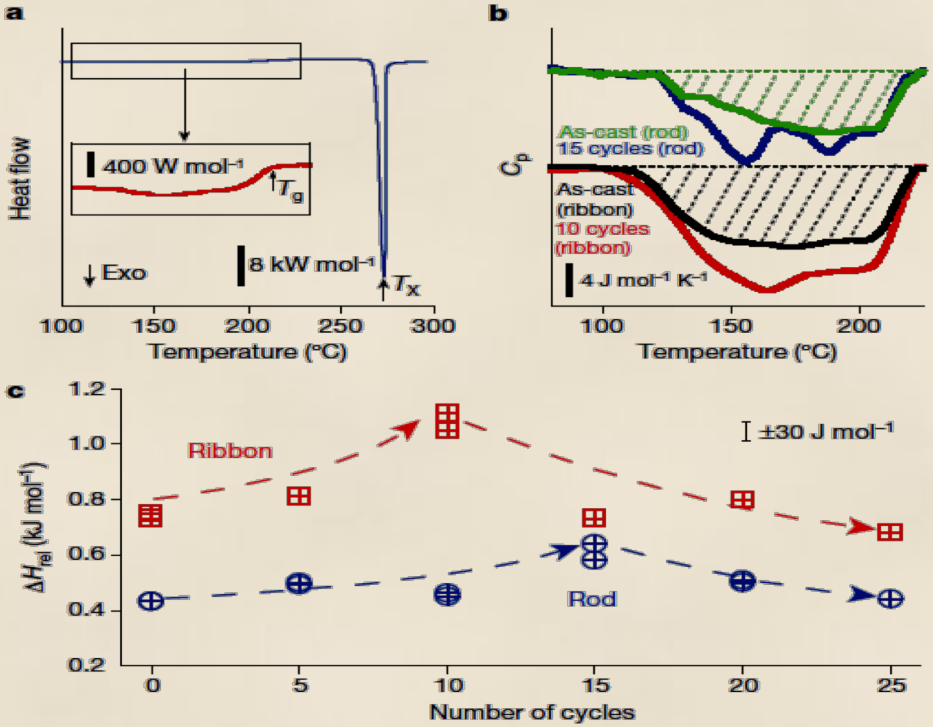

Figure 2 | Differential scanning calorimetry (DSC) of melt-spun ribbons of $La_{55}Ni_{20}Al_{25}$ and bulk rods of $La_{55}Ni_{10}Al_{35}$ metallic glasses.

Summary

- The structure of melts/liquids/glasses is usually studied by X-ray and n-diffraction while glasses can also be studied by TEM, AFM and STM techniques.
- In-situ vitrification of the liquid alloys reveal atomic structural changes in the supercooled regime showed that when the liquid alloy is supercooled, it shows an expansion instead of a contraction of the 1st coordination shell between the liquidus T_l and the glass transition T_g, corresponding to an increase in the nearest interatomic distances. These changes are consistent with the temperature evolution of the TSRO and CSRO.
- At the same time the maximum of the 2nd coordination shell moves to lower distances as expected from thermal contraction. Below T_g the metallic glassy solid contracts/expands in a usual way according to thermal vibrations.
- On supercooling, the relative integrated intensity of a low-R subpeak (P1) of the 1st coordination shell in the PDF of the $Pd_{42.5}Cu_{30}Ni_{7.5}P_{20}$ alloy becomes stronger on cooling from the melt to T_g. The increase in the sub-peak intensity suggests formation of atomic clusters with P at the center and Ni and Cu at the nearest neighbor that are bonded to P covalently during supercooling of the melt. This is the reason for liquid fragility.


Thank you very
much for your
attention
WESTIN